SUSTAINABLE CONVERSION OF AGRO-WASTES INTO VALUABLE PRODUCTS USING INEXPENSIVE NANO-CATALYST

Thesis

Submitted By:

Aritro Sarkar

Exam Roll No.: M4CHE22006
Class Roll No.: 002010302006

Reg. No.: 153943 of 2020-2021

Under the guidance of:

Prof. Rajat Chakraborty

A Thesis submitted in the fulfilment of the requirement for the degree of

MASTERS IN CHEMICAL ENGINEERING

DEPARTMENT OF CHEMICAL ENGINEERING

Jadavpur University

Jadavpur, Kolkata-700032

JULY, 2022

Declaration of Originality and Compliance of Academic Ethics

I hereby declare that this thesis contains literature survey and original research work by the undersigned candidate, as part of his "Master of Chemical Engineering" studies. All information in this document have been obtained and presented in accordance with academic rules and ethical conduct. I also declare that, as required by these rules and conduct, I have fully cited and referenced all material and results that are not original to this work.

Name: **Aritro Sarkar**

Exam Roll No.: **M4CHE22006**

Thesis Title:

SUSTAINABLE CONVERSION OF AGRO-WASTES INTO VALUABLE PRODUCTS USING INEXPENSIVE NANO-CATALYST.

Signature:

Date:

July 2022

Certification

This is to certify that Mr. Aritro Sarkar, final year Masters of Chemical Engineering (M.E) examination student of the Department of Chemical Engineering, Jadavpur University (Exam Roll No.: M4CHE22006; Reg. No.:153943 of 2020-2021 has completed the project titled: - **"SUSTAINABLE CONVERSION OF AGRO-WASTES INTO VALUABLE PRODUCTS USING INEXPENSIVE NANO-CATALYST"**, *under the guidance of Prof. Rajat Chakraborty during his Masters Curriculum. This work has not been reported earlier anywhere and can be approved for submission in partial fulfillment of the coarse work.*

Prof. Rajat Chakraborty

Head of Department and Professor,
Chemical Engineering Department,
Jadavpur University.

Prof. Rajat Chakraborty

Project Supervisor and Professor,
Chemical Engineering Department,
Jadavpur University.

Prof. Chandan Mazumdar

Dean of Faculty and Engineering Technology,
Jadavpur University.

Acknowledgement

In preparing this thesis, I have worked with a great number of people whose contribution in assorted ways to the research and the making of the thesis deserved special mention. It is a pleasure to convey my gratitude to them all in my humble acknowledgment.

In the first place I would like to record my gratitude to Prof. Rajat Chakraborty, Head of Department and Project Supervisor, for his supervision, advice and guidance from the very early stage of this research as well as giving me extraordinary experiences throughout the work. Above all and the most needed, he provided me unflinching encouragement and support in various ways.

I am very grateful to all other faculty members for their help and cooperation. I would also like to offer my acknowledgements to staff members of my department. I am also indebted to Jadavpur University, Dept. of Chemical Engineering for support and giving me the opportunity to use the equipment's to do my research.

I am very much thankful to my PhD senior Mr. Sourav Barman for his continuous support, valuable guidance and encouragement at various stages of the project period. My fellow friends should also be recognized for their support. My sincere appreciation also extends to all my colleagues and others who have provided assistance at various occasions. Their views and tips are useful indeed. Unfortunately, it is not possible to list all of them in this limited space.

Finally I would like to thank to my family for their excellent support and try to keep me high spirited throughout the master degree programme.

Table of Contents

Chapter 1

ABSTRACT

1.1 Abstract

A systematic investigation employing wasted printed circuit boards (W-PCB) derived silica-alumina based glass fiber (GF) support grafted with molybdenum oxide and gallium oxynitrate catalyst (GaMo-GF) have been synthesized and studied for photocatalytic-hydrolysis of delignified corncob (DCC) to reducing sugars (RS) in a quartz halogen solar batch reactor(QHSR). Corncob was delignified by peroxide-acetic acid treatment. The highest RS yield obtained from DCC (cellulose 75.14%, hemicellulose 22.65% and lignin 2.1%) by using the said catalyst was 72.47% (at 100ºC for 20 mins of reaction time and 15 wt. % catalyst). On contrary at the same condition the traditionally heated reactor (THR) gave a low yield of 25.58%. The optimum GaMo-GF catalyst was found to have a surface area of 28.008 m^2/g, high pore volume (0.04198 cc/g) & high pore diameter (13.5872 nm), respectively, according to BET analysis. Furthermore, MoO_3 and GaON crystalline phases were also detected by XRD and the presence of gallium and molybdenum has been confirmed by FTIR analysis. The band gap of the synthesized catalyst was found to be 2.3eV through UV-Vis-NIR spectroscopy. Using the openLCA platform (ecoinvent database v3.8), the process' overall environmental sustainability was evaluated. The QHSR response was significantly more ecologically benign than the THR reaction having over 50% lower harmful environmental impacts. Moreover, the QHSR proved to be more than 90% energy efficient than THR.

1.2 Research Highlights

- Sustainable delignified corncob conversion by waste printed circuit board based photo-catalyst.
- High reducing sugar yield (72.47%) achieved by W-PCB based GaON/MoO_3 catalyst.
- Photocatalytic hydrolysis of delignified corncob under visible radiation.
- QHSR based reaction had a 57.7% lower GWE100 than THR based reaction.
- The cost of 1kg of optimum GaMo-GF catalyst was INR 388.85

Chapter 2

INTRODUCTION

2.1 Introduction

Renewable energy is one of the paths to achieve environmental and societal sustainability. For a longer length of time, renewable energy sources gifts us with considerably cleaner and greener energy. In comparison to a fossil fuel source, it creates less pollutants and emissions. Renewable energy sources have been discovered by

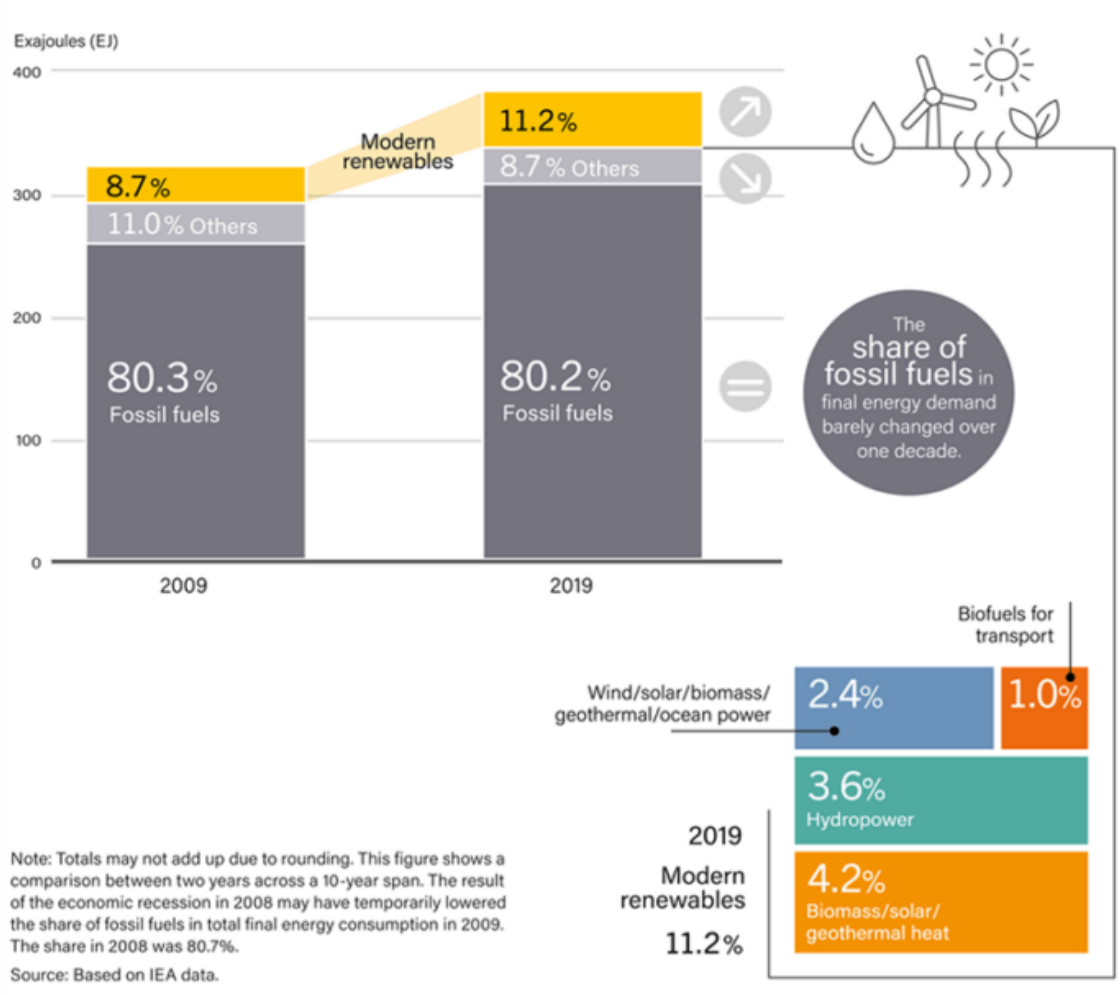

Figure 1: Estimated Global Renewable Energy Share of Total Final Energy Consumption (2009-2019)

scientists all over the world to be considerably more sustainable, providing a wide range of applications as well as job opportunities for local populations. It's also capable of ensuring a country's energy security. From Figure 1 it can be seen that globally, contemporary renewables (biomass, geothermal, solar, hydro, wind, and biofuels) provided around 11.2 percent of the energy utilized for heating, electricity, and

transportation in 2019, up from 8.7 percent a decade ago. By the conclusion of the year 2020, renewable energy accounted for 29% of worldwide power generation. Well over 256 GW of capacity was added in 2020, driven by wind and solar PV, representing an almost 10% increase in overall installed renewable power capacity.

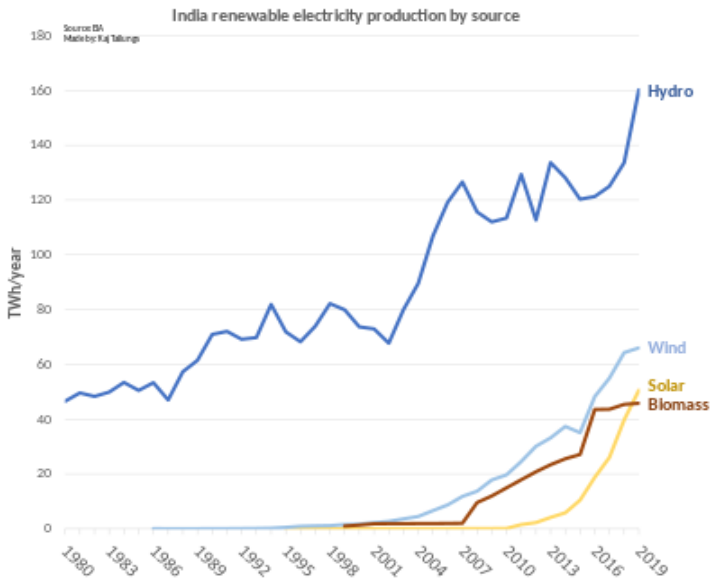

Figure 2: Sources of India's renewable electricity production

India is the world's third largest power user and third largest renewable energy producer, with renewable energy accounting for 38% of energy capacity constructed in 2020 (136 GW of 373 GW). According to Ernst & Young's (EY) 2021 Renewable Energy Country Attractiveness Index (RECAI), India is rated third, behind the United States and China. India had a renewable energy production of 150 GW in November 2021, which included solar, wind, small hydro power, bio-mass, big hydro and nuclear.

India has committed to a target of 450 GW of renewable energy capacity by 2030. It may be shown from Figure 2 that majority of the renewable energy in India comes from hydro power but since 2007 energy generation from biomass has increased significantly. Biomass can be converted into biofuels (bioethanol and biodiesel) that may be blended with current vehicle fuels. As per the Biofuels Report[1], India is now blending roughly 8.1 percent bioethanol in gasoline, with the number predicted to rise to 20 percent by 2025 by the Government of India. The Union government has increased its commitment to 1G biofuels in order to facilitate a speedier transition. Food grains, such as maize and excess rice from Food Corporation of India (FCI) reserves, have been authorized in addition to sugar-based manufacturing. In addition, the policy focuses on boosting study in 2G technologies (from waste biomass) as an establishing long-term sustainable solutions. However, India generates just 12 terawatt-hours of biofuel energy, whereas the worldwide total is over 1043 terawatt-hours, as can be seen in Figure 3. As a result, India's biofuel needs must be met mostly through imports[2].

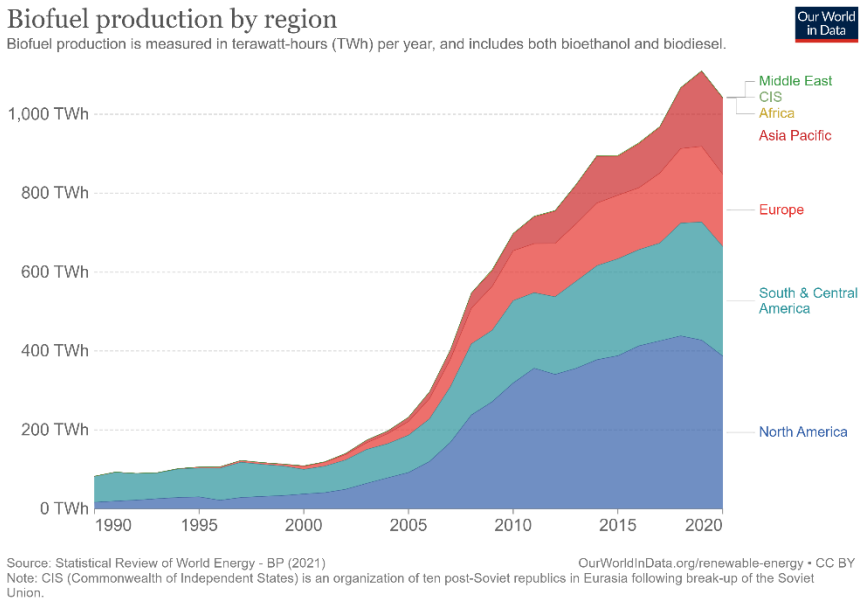

Figure 3: Global biofuel production data

As a result, it is critical to look for alternative, low-cost, and easily available feedstock for renewable energy generation. Biomasses are an example of a feedstock that has an infinite supply and is very inexpensive.

Every year, photosynthesis generates around hundred and fifty billion tons of biomass, of which people use just 3–4 percent of the total for eating and non-food purposes [3]. Low-value farming and forest byproducts, plants, and energy crops are excellent biomass sources for producing bio-products from a technological and socio-economic viewpoint since the biomass feedstock does not compete with the food chain. Lignocellulosic biomass (LB) is a plentiful and renewable resource made up mostly of polysaccharides (cellulose and hemicelluloses) and an aromatic polymer derived from plants (lignin). Without jeopardising global food security, LB has a great potential as a substitute for fossil resources in the production of 2nd generation of biofuels, bio-sourced chemicals, and materials [4]. Moreover, multiple studies have demonstrated that using LB as a feedstock results in low pollution emissions [5,6]. The three types of lignocellulosic biomass are virgin biomass, waste biomass, and energy crops. All naturally existing terrestrial plants, such as trees, shrubs, and grass, are considered virgin biomass. Waste biomass is generated as a low-value by-product in a variety of industries, including agriculture (corn stover, sugarcane bagasse, straw, and so on) and forestry (saw mill and paper mill discards). Switchgrass (Panicum virgatum) and Elephant grass are examples of energy crops with large yields of lignocellulosic biomass that may be used as a raw material for the manufacture of second-generation biofuels.

Cellulose [$(C_6H_{10}O_5)_n$] is the most common biopolymer on the planet. It's a polysaccharide, or complex carbohydrate, made up of hundreds or even thousands of glucose units linked together in a chain. Cellulose is formed when D-glucose units

establish β-(1→4)-glycosidic linkages (Figure 4). Starch and glycogen, on the other hand, are formed by the formation of α-(1→4)-glycosidic bonds with glucose molecules. Because of its connections, cellulose is a straight chain polymer. The hydroxyl groups on glucose molecules generate hydrogen bonds with O_2 atoms, which hold the chains in place and give the fibers a high tensile strength. The crystallinity of cellulose is also due to this cause. Cellulose is insoluble in polar solvents such as water and many other organic solvents, but soluble in a variety of ionic liquids. It's a chiral structure with a significant affinity for water, making it hydrophilic, and has a contact angle of 20-30 degrees.

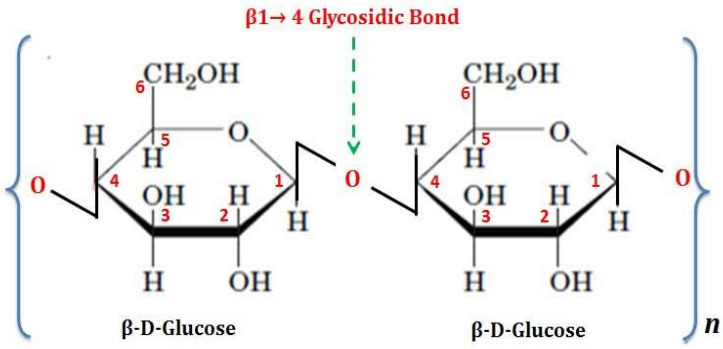

Figure 4: Structure of Cellulose

In the fields of paper and pulp, medicines, clothing, and electronics, cellulose has several potential applications. The kraft method […] is used to extract cellulose from lignin in paper manufacturing industry, which is the most common industrial application for cellulose. In the textile business, cellulose fibers are used. To create rayon, cotton and other plant fibers can be utilized directly or processed. Microcrystalline and powdered cellulose are employed in food additives as well as medication fillers. Fluid filtration as well as thin layer chromatography are two

applications of cellulose used by scientists. The transformer's insulation and cables are also made of cellulose. Because cellulose is a D-glucose polymer, the production of bio ethanol is a primary reason for its international appeal. With fossil fuel reserves depleting and pollution from car emissions rising, bioethanol is a great fuel additive that tackles two problems at once. It is responsible for lower emissions and, by blending with gasoline, it is able to fulfil rising fuel demand. Other useful platform chemicals generated from cellulose include fructose, glucose, Hydroxymethylfurfural (5-HMF), and LA (Levulinic Acid), in addition to ethanol. When cellulose is hydrolyzed in the presence of an acidic or ionic solution, reducing sugars are produced (RS). Total reducing sugars (TRS) are made up of all monosaccharides as well as certain polysaccharides. Monosaccharide RS include glucose, fructose, galactose, and xylose, whereas disaccharide RS include lactose and maltose. RS is any sugar with a free aldehyde or ketone group that may reduce a variety of reagents, including Tollens and 3, 5-dinitrosalicylic acid. RS is a helpful platform chemical that may be used to make a variety of useful compounds.

Hemicellulose is a hetero polymer found in the cell wall of plants, alongside cellulose. It is primarily amorphous in form, unlike cellulose, and has very little tensile strength. Hemicellulose is a branching structure that, through hydrogen bonding and van der Waals forces, provides an interpenetrating matrix for cellulose. Hemicellulose is easier to hydrolyze than cellulose. Hemicellulose is mainly made up of xylan, but it

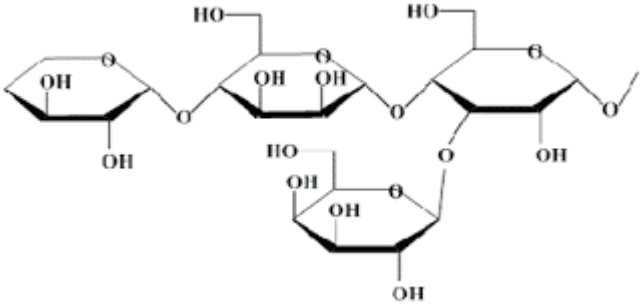

Figure 5: Structure of Hemicellulose

also contains arabinan, galactan, and mannan, and its fundamental structure is a linear backbone of β-(1→4) linked D-xylopyranosyl residues. Although xylose is mostly found as the monomer of hemicellulose, other biomasses, such as softwood, have mannose as the primary sugar molecule. Figure 5 depicts a typical hemicellulose structural unit including mono saccharides such as xylose, mannose, & galactose.

Commercially, hemicelluloses are important. Guar & galactomannans, tamarind gum are all examples of seed storage hemicelluloses that are utilized directly as food goods (xyloglucan)[7]. Hemicelluloses also provide many food and feed products essential qualities. The insoluble arabinoxylans have an impact on baking quality in the baking business. The USFDA recommends daily use of β-(1→3, 1→4)-glucans since it has been shown to decrease cholesterol in hypercholesterolemic people[8]. The creation of xylose is caused by the hydrolysis of hemicellulose. Xylose is a key platform chemical that is used to make a variety of other compounds. A number of studies have been conducted on the efficient on-pot production of furfural from xylose. Further transformation of furfural over acid catalysts can provide levulinate esters. Another major molecule used as a sugar replacement is xylitol, which is made from hemicellulose by fermentation.

Lignin is an oxygen containing natural polymer that, together with cellulose, is the most important component of wood. Lignin is a combination of three complicated polymeric molecules and is a phenolic chemical (one with a —OH group connected to an aromatic ring, Figure 6). Whether the lignin comes from gymnosperms, woody angiosperms, or grasses determines the proportional amounts of each of the three

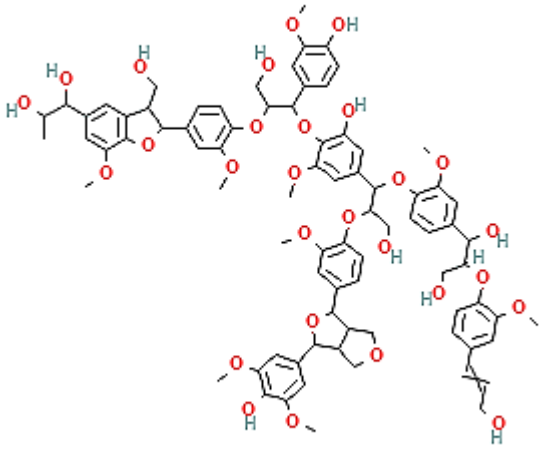

Figure 6: Structure of Lignin

monomers. Lignin is a molecule that is cross-linked to cellulose and hemicellulose via hydrogen bonds, ionic interactions, ester and ether linkages, and van der Waals interactions. The presence of lignin in lignocelluloses creates a protective barrier that keeps plant cells from being destroyed. Lignin additionally waterproofs the cell wall, allowing water to move upward in the xylem tissues. Lastly, lignin has antifungal characteristics and is frequently accumulated in response to fungus harm, shielding the plant body from fungal enzymes and poisons.

Lignin is a component of lignocellulosic biomass that may be degraded using appropriate catalysts to produce a variety of useful compounds such as vanillin, vanillic acid, and syringaldehyde[9].

Different lignocellulosic biomass has different composition of cellulose, hemicellulose and lignin. Table 1 shows the compositional analysis of various biomass, including the % cellulose, hemicellulose, and lignin content.

Table 1: Compositional analysis of different lignocellulosic biomass

Lignocellulosic Biomass	**Cellulose**	**Hemicellulose**	**Lignin**	**Reference**
Sugarcane top	29.7	18.9	25.8	[10]
Bagasse	29.9	35.1	18.2	[11]
Sugarcane Bagasse	44.1	26.9	24.1	[12]
Sweet Sorghum Bagasse	37	18	19.8	[13]
Wheat Straw	39	18.7	17.1	[14]
Rice Straw	35.9	21.1	24.2	[15]
Corn Stover	36.5	31.6	17.2	[16]
Corn Stalk	34.52	27.6	21.2	[17,18]
Corn Cob	32.64	31.8	17	[19]
Pine	47	20.3	27.3	[20]
Birch	47.1	26	22.2	[20]
Perennial grass	50.4	24.9	12.2	[21]

Understanding the conversion process is important since the main goal of this present effort is to convert biomass-derived cellulose into sugar molecules. Hydrolysis

is a process that may breakdown both cellulose and hemicellulose into its monomeric components. The presence of water causes the breaking of holocellulose polymers. Acid hydrolysis and enzyme hydrolysis are the two main kinds of cellulose hydrolysis. The, β-(1→4) glycosidic connections are broken down by water molecules in dilute or intense acid hydrolysis, resulting in disintegration of the cellulose polymers into D-glucose units. When cellulose is hydrolyzed with a hot concentrated acid, hydrocellulose is converted to simple polysaccharides, which are subsequently converted to monosaccharides. Enzymatic hydrolysis of cellulose, on the other hand, happens in a bioreactor, primarily in the presence of an enzyme such as cellulase. A typical method is to use enzymes to break down cellulose and then ferment it into bioethanol. However, the enzymatic pathway takes a long time and is prone to inhibitors.

2.2 Electronic Waste

Electrical & electronic equipment is becoming a need in modern society. Because of its broad availability and use, it has enabled a large portion of the world's population to enjoy greater living standards. The way we manufacture, use, and dispose of e-waste, on the other hand, is unsustainable. Externalities – such as resource consumption, greenhouse gas emissions, and hazardous material release during informal recycling methods – highlight the challenge of staying below sustainable limitations due to the sluggish adoption of collecting and recycling. Globally, 44.7 million metric tons of e-waste were created in 2019 which is expected to reach 74 metric tons by the year 2030, according to the Global E-waste Monitor-2020 [22]. The intrinsic components of electronic trash, discarded printed circuit boards (PCBs), account for around 3% of e-waste [23]. Hazardous compounds in waste PCB(W-PCB), including as heavy metals, carcinogenic brominated flame retardants, and polyvinyl chloride, pose

a risk to the environment and humans [24,25]. The current system is challenged with poor recovery and recycling rates. Even countries that have established a systematic e-waste management system face the same problem. Only 17.4 percent of the world's 53.6 million metric tonnes (Mt) of waste was officially recognized as appropriately collected & recycled in 2019. Since 2014, it has grown by 1.8 Mt, but overall e-waste creation has climbed by 9.2 Mt. This suggests that recycling efforts aren't keeping up with the global increase in e-waste.

The necessity of efficient e-waste management is becoming recognized throughout the South Asian area. In Southern Asia, India seems to be the only country having e-waste law, however numerous other countries are contemplating it. Only licensed dismantlers & recyclers are allowed to collect e-waste in India, which has been the case since 2011. The E-Waste (Management) Rules 2016 include provisions for a producer, distributor, refurbisher & Producer Responsibility Organization (PRO). In the framework of extracting various secondary sources from e-waste, the National Resources Policy envisions producers playing a significant role.

Recycling of W-PCB is gaining popularity across the world, since it promotes environmental preservation and long-term growth. W-PCB is referred to as "urban mines"[26] because of its plentiful resources (about 30% metals and 70% nonmetals). Extraction of precious metals from W-PCB has been a widespread procedure due to the inherent financial and economic incentives. In the last several decades, many separation procedures of metal and nonmetallic constituents of W-PCBs, such as physical processes[27], thermal processing[28,29], hydrometallurgical processing[30], and solvent extraction[31], have been documented. Because of the limitations of present technology, new solutions are still required for effective W-PCB recycling.

2.3 Use of catalyst in reaction

Catalysts play a crucial role in chemical reactions. Negative catalysis are crucial for stopping any chain reaction, but positive catalysis can accelerate the process's pace by lowering the activation energy. Homogeneous and heterogeneous catalysts are the two categories into which catalysts fall. A homogeneous catalyst is one whose phase matches that of the molecules in the reactant. Heterogeneous catalysts, in contrast, have a distinct phase than the reactants. Due to their difficulties in isolating out from product stream, homogeneous catalysts really aren't commonly employed in industrial processes nowadays. Difficult recycling and expensive effluent treatment are some further downsides. Acidic homogeneous catalysts can leave a soapy film on the product streams and are corrosive to the reactors. The reactant molecules bind to the active site of heterogeneous catalysts in an intermediate manner, causing the reaction to take place. The majority of heterogeneous catalysts combine an active site and support by doping the catalytic component across an appropriate support surface. By doing so, the catalyst's cost is decreased and its effectiveness is increased. To increase the surface area in a certain reaction to occur, catalyst supports are mostly composed of porous materials. Zeolite, activated carbon, as well as alumina are some of the often employed support materials. Recent developments have demonstrated the employment of specialized supports in the creation of different catalysts, including silica, titanium dioxide, calcium carbonate, etc. The number of available active sites is decreased because a support material stops the catalyst from piling up and forming a composite. A support also helps to lessen the sintering issue. Supports have been demonstrated in several experiments to have improved the surface area of a catalyst as a whole. Doping catalysts over a support is economically advantageous since it lowers the cost of the catalyst overall because support materials are often less expensive than the pricey

catalysts. Supports thereby provide the catalytic system more activity. Another method of accelerating a process is photo-catalysis, in which the catalyst is activated in the presence of photons. When the catalysts are exposed to enough radiation, the electrons from the valence band leap across the impermissible energy gap and into the conduction band. An electron-hole pair is thus produced. Following their separation from one another, the electron-hole pair moves in opposing directions toward the catalyst's surface. In such a possible reaction system, those charges are used.

Titania (TiO_2) is one of the often utilised photocatalysts. Three different forms—anatase, brookite & rutile—can be found in nature. Titania's metastable variant is called Anatase. While brookite has an orthorhombic crystal structure, anatase and rutile both have tetragonal crystal structures. The rutile phase is created when anatase and brookite are heated over 600°C by a process known as rearrangement. Under equilibrium, the rutile phase develops[32]. When ultraviolet light (10–400 nm) is present, nano TiO_2 (NaT) is activated. However, there is evidence that TiO_2 can photocatalyze in visible light when doped with metal oxides or nitrogen ions[33]. When anatase TiO_2 is exposed to certain wavelength light (10-400nm), an electron (e^-) moves from the valence band to the conduction band and subsequently departs the atom, forming a hole (h^+). Whereas the hole may oxidise another material, the electron can only decrease one substance. This method, which was first applied in 1967 to divide water molecules, is

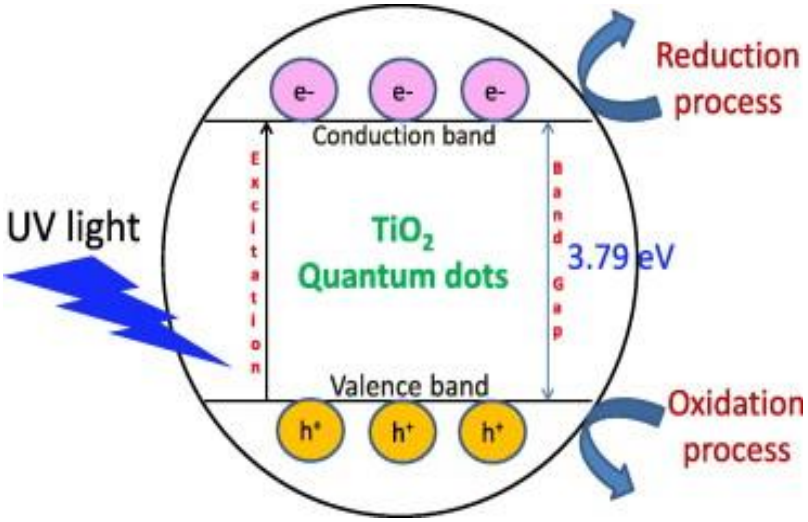

Figure 7: Photocatalytic activity of TiO_2

known as the Honda Fujishima effect[34]. TiO_2 functions as a photocatalyst, as seen in Figure 7.

Another kind of heterogeneous catalyst is the solid acid catalyst. The acid catalyst gives proton (H^+), in accordance with the Bronsted-Lowry acid base hypothesis. Proton transfer is what causes typical acid catalysis to happen. Silico-aluminates, sulfated zirconia, sulfonated polystyrene, and other materials are used as commercial acid catalysts. Amberlyst-15 (A15) is yet another commercially accessible solid acid catalyst with highly selective characteristics and a low environmental impact. A15 is a resin structure that resembles a reticulated net. It is just a polystyrene compound with a sulphonic group that, thanks to its exceptional protonation characteristic, supplies the acidity. Figure 8 depicts the A15 catalyst's structural formula. A15 may be recycled and used again and is simpler to remove from the reaction mixture. Numerous organic reactions, including as Friedal craft,

transesterification, crossing aldol condensation, Michael addition, etc., have been successfully completed by A15 catalyst, according to literature [35].

Additionally, studies have demonstrated how sulfonated acid catalysts provide a better conversion rate of cellulose into glucose than the zeolite catalyst [36]. For a number of reasons, the d-block components exhibit remarkable catalytic characteristics. Their own catalytic activity is aided by the unoccupied d-orbital. Additionally, the existence of unpaired electrons on the outermost shell of the atoms (apart from Cu and Zn) aids with the catalytic activity. The hydrolysis of cellulose has been shown to be improved by the oxides of various d-block elements[37,38].

Non-ionizing radiation heating systems are now more energy-efficient and quicker for a variety of processes. The energy required for bond stretching as well as bonding vibration is transmitted uniformly via radiation[39,40]. For these reasons, radiation has generally been favored to traditional heating. Non-ionizing radiation does not ionise the atoms and delivers sufficient energy for bond excitation. Non-ionising radiations, when used properly, do not impact human health in the same way as ionising

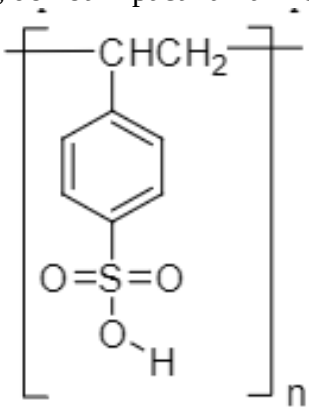

Figure 8: Structure of Amberlyst-15

radiations do, which are extremely dangerous. Compared to ionising rays, they have a lower frequency and a longer wavelength. Ionizing radiations include gamma and x-rays, whereas non-ionizing radiations include microwave, ultraviolet, visible, infrared,

and radio waves. Although several hydrolysis processes have been performed in the presence of microwave and infrared radiation, no literature has been documented where a combination of various radiations of various wavelengths is used at the same time.

Chapter 3

LITERATURE REVIEW

3.1 Biomass to platform chemicals

There is a global energy issue that has to be addressed. With the depletion of fossil fuel reserves, gasoline is being blended with biofuel. Bioethanol, 5-HMF, ethyl levulinate, levulinic acid (LA) and reducing sugar are some of the important compounds used in fuel blenders. These platform chemicals are derived from biomass because of their large supply and low cost. Lignocellulosic biomass comprises cellulose and hemicellulose, which may be transformed into a variety of C5, C6 compounds of commercial value. The following literatures show the synthesis of many value-added compounds (mainly reducing sugar) from cellulose or non-food Lignocellulosic biomass, which might help reduce the world's rapidly dwindling fossil fuel reserve.

3.1.1 Non-heterogeneous Catalyst

- **Camesasca et al.**[41]:-Napiergrass was employed as feed for bioethanol extraction in this study. Napiergrass seems to be a non-food plant that has gained popularity due to its appealing yield and environmentally friendly growing methods. To get the sugar product, dilute H_2SO_4 was used to hydrolyze the feed. The acid hydrolyzed sugar was fermented with a yeast microbe (Pichia stipitis) for 176 hours, yielding an ethyl alcohol concentration of 21 g/L. A similar alkaline pretreatment was also investigated, in which the feedstock was exposed to caustic soda alkalization (under 80 ° C for 6 hours), which effectively enhanced lignin removal. Using the enzyme -glucosidase plus polyethylene glycol 6000, the greatest product concentration of 24g/L was achieved. Enzymatic hydrolysis utilizing the NREL technique and the cellulase complex NS50013 yielded a 24 percent lower ethanol. The conversion time for the

fermentation process was obviously substantially longer. The 6 hour alkalization time will use a lot of energy, making the procedure inefficient.

- **Liu et al.**[42]**:-** According to the literature, rapid pyrolysis of a plant mass was used to accomplish selective breakdown of LB into fuel. This procedure was said to be very effective and cost-effective. Fast pyrolysis seems to be a novel technology that involves quickly heating organic materials to high temperatures in the absence of air. Organic vapors, pyro gases, and charcoal are created during this process. Bio-oil is created by condensing the vapors. The oils produced by this technique are hydrocarbon-based. They have a high calorific value, making them commercially valuable. The biomass was pyrolyzed using a catalyst in this procedure. It's also difficult to make such effective catalysts. During the pyrolysis process, the oil absorbs a higher amount of oxygen, resulting in the formation of various oxygenates. This property came with a number of drawbacks for the oil, including poor heating value, high viscosity, high corrosiveness and instability. In addition, no appropriate methods for separating various fuels (like diesel, gasoline & ATF) in a cost-effective manner were discovered in this literature.

- **Mittal et al.**[43]**:-** The main goal of this research was to increase furfural production by using a microwave reactor to directly dehydrate untreated biomass, eliminating the need for expensive unit operations like pretreatment and enzymatic hydrolysis, that are otherwise needed for the breakup of polymeric sugars to monomeric forms (glucose and xylose). Hydrolysis of different biomasses such as loblolly pine, corn stover, hybrid poplar and switch

grass have been conducted in this study. Among these biomasses hybrid poplar gave the highest combined furfural (furfural & HMF) yield of 75%. HMF & furfural yields were shown to be predominantly reliant on hexosan & pentosan loading, independent of feedstock type. The highest yield was obtained at 200ºC and 5 minutes of reaction time using 33mM of HCL and 8mM of $AlCl_3$ in a dioxane plus water solvent solution in a 4:1 ratio. There was no discernible influence of crystallinity as well as lignin concentration on furfurals production.

- **Hermiati et al.**[44]**:** Cassava pulp was hydrolyzed with the help of oxalic acid under microwave radiation. A cassava pulp suspension in 0.5 % of $(COOH)_2$ (1 g/20 mL) was microwaved for 5 minutes between 140-230°C, with 4 minutes pre-heating. The maximum glucose yield (78 %) was achieved following hydrolysis at 180°C without the addition of activated carbon. The glucose collected can then be fermented further to make bioethanol for fuel. The addition of activated carbon to the hydrolysis of cassava pulp in oxalic acid medium under radiation resulted in a lighter coloured saccharified solution with no influence on glucose production.

- **Lenihan et al.**[45]**:** The hydrolysis of potato peel in a pressurized batch reactor utilizing dilute H_3PO_4 (phosphoric acid) has been investigated. The cellulose concentration of potato peel is quite high, at 55.25 %. Hemicellulose (11.71 %) and lignin (14.24 %) concentrations, on the other hand, were determined to be quite low. Milled potato peels (1mm diameter) were added to the reactor followed by the addition of dilute phosphoric acid. The reactor was then pressurized to 20 bar with the help of nitrogen. Then the temperature was

increased to the desired value. Under ideal conditions, a total sugar yield of 82.5 % was reached. At 135°C & 10% (w/w) acid content, the best yield was attained. After 8 minutes, 55.2 g sugar/100 g potato peel is generated. Because of its low cost and high sugar yields, potato peel appears to be a viable alternative as a feed material for the generation of sugars for biofuel synthesis.

- **Kupiainen et al.**[46]**:** To delignify lignocellulosic crop wastes for pulp manufacture or to pre-treat them before enzymatic hydrolysis for bioethanol production, organosolv techniques can be utilized. To create glucose, an organic solvent was utilized like an acidic catalyst in this work. Hydrolysis studies were conducted out at 180–220 °C in 5–20 % formic acid. The basic material was wheat straw pulp that had been delignified using the formicodeli technique. The yields of glucose from pulp (40%) were found to be substantially greater than those from MCC (22%) at a following reaction condition: temperature 200ºC and time 7 min, a standard material for cellulose hydrolysis. The findings show that cellulose hydrolysis in actual fibers is more selective for glucose than cellulose hydrolysis in microcrystalline cellulose particles.
- **Yu et al.**[47]: This literature has used waste paper fiber to extract cellulose and then convert it into a glucose component by enzymatic hydrolysis. Furthermore, the study discovered that the presence of Cationic polymers improves the enzymatic hydrolysis of waste paper fibers. Polyethyleneimine outperformed cationic polyacrylamide and cationic starch in producing a total sugar content of 73.9 g/L. The enzymatic hydrolysis was performed in a 100mL polytetrafluoroethylene reactor with a shaft for homogeneous mixing. Initially,

a cellulase loading of 18FPU per gramme of cellulose and a betaglucosidase loading of 25CBU per gramme of cellulose were used. The reaction temperature was held constant at 48°C, and the pH was set at 4.8. It was also discovered that the addition of cationic polymer reduces the need for cellulase.

- **Assabjeu et al.:** This research sought to improve the enzymatic hydrolysis of cellulose generated from Triplochiton scleroxylon, also known as the Ayous plant's sawdust. 53 percent of the processed and delignified sawdust is cellulose, which is a significant proportion. The cellulose was hydrolyzed by enzymes to form Dglucose, which fermented to make ethanol. Three factors—amount of substrate, amount of enzyme, and reaction time—were used to optimise the hydrolysis reaction. The 72-hour time frame, 9.07 percent substrate concentration, and 21.36 units of enzyme loading were shown to represent the reaction's ideal conditions. Up to a 69 percent yield of reducing sugars might be produced using the cellulose extracted from sawdust. The amount of decreasing sugar seen per millilitre was 21.88mg. According to an individual impact research, excessive substrate loading degrades the yield, but increased enzyme loading and duration are advantageous.

3.1.2 Heterogeneous Catalyst

- **Wu et al.**[48]**:** In this work a biochar based sulfonic acid catalyst (BC-SO_3H) has been prepared to study the hydrolysis of cellulose. To create a carbonized solid, 20 g of bamboo powder has been treated with 80% H_2SO_4 (100 ml) at 80ºC for 3 hours. The ground substance (10.5 g) was then submerged in 150 mL oleum (50 wt% SO_3) & heated to 80ºC under N_2 for 2 hours. The cooled suspension

was filtered after sulfonation to produce a dark precipitate. Finally the black precipitate was washed with hot water followed by drying. Under optimal condition (0.2g microcrystalline cellulose, 0.1g BC-SO_3H, 90ºC, 60 min) utilizing microwave irradiation gave a maximum glucose yield of 19.8%. The BC-SO_3H acid had a much higher turnover number (1.34-1.7) than dil. sulphuric acid (0.02), this was most likely owing to their great attraction for cellulose's β-(1→4) glycosidic linkages. Furthermore, microwave irradiation had an important function in energizing cellulose molecules and intensifying particle collisions, which might result in a significant acceleration impact upon the highly heterogeneous catalytic process.

- **Jiang et al.**[49]**:** Corncob has been hydrolysed by a carbon based (from residue of hydrolysis) solid acid (CSA) catalyst. These CSA catalysts was made from hydrolyzed corncob waste left over from xylose synthesis. The dried hydrolyzed residue (20 g) is heated for 5 hours at 450ºC under N_2 flow to produce brown carbon compounds, which were then ground to powder in a conventional synthesis. To introduce SO_3H into the surface of carbon, the powder (2 g) has been heated in 60 mL fuming sulphuric acid (20% SO_3) at 120 °C for 10 hours. The suspension was then filtered followed by washing with hot water. Before the reaction, the CSA was then dried for 24 hours at 105ºC and ground for 30 minutes in a mortar. Corncob hydrolysis was performed in a microwave reactor. A maximum glucose yield of 34.6% was obtained at 130ºC and 60 mins of reaction time where the catalyst to feed ratio was 1:1 with water as the sole solvent. The CSA may be made from solid waste from hydrolyzed biomass

residue, which not only fully uses the unconverted component of lignocellulosic biomass and lowers CSA costs, but also minimises pollution.

- **Onda et al.**[36]**:** Ball milled cellulose has been reacted with prepared sulfonated carbon (activated) catalyst ($ACSO_3H$) to produce glucose. Activated carbon (1.0 g) was typically added to conc. sulphuric acid (18 mol L^{-1}, 20 mL) and heated for 16 hours at 150ºC under Ar flow (40 mL min-1). The $ACSO_3H$ that resulted was repeatedly rinsed with hot DI water at 80ºC. To avoid elution of SO_4^{2-} ions in hydrothermal reaction medium at 150ºC, the black powder was then hydrothermally pre-treated at 200ºC for 3 h and afterwards washed again with hot DI water until no sulphate ions were identified in the wash water. The following was the reaction procedure: cellulose (45 mg) was ball-milled for 48 hours, catalyst (50 mg), and water (5.0 mL) were added to a steal autoclave walled with Teflon (25 mL) under air. With agitation, the autoclave had been heated to 150ºC for 24 hours (22 rpm). The reaction mix was filtered after the reaction & the filtrate was examined. At the above mentioned condition a maximum glucose yield of 40.5% was obtained. But such a high reaction time and high temperature makes the process non-viable.

- **Shuai et al.**[50]**:** In this study, sulfonated chloromethyl polystyrene resin (CP-SO_3H), a new cellulase-mimetic solid catalyst with binding sites for cellulose (–Cl) and catalytic active sites (–SO_3H), was produced for cellulose degradation. The catalyst prefers oligosaccharides over those monosaccharides because the former have more hydroxyl groups capable of forming H+ bonds with said –Cl groups on the catalyst that is critical and important to keep the cellulose

hydrolysis going, adsorbing the substrate & desorbing the product continuously. Starch plus crystalline cellulose were all hydrolyzed by the catalyst. A 91% glucose yield was obtained from 0.1g of cellulose by utilizing 0.25g of CP-SO_3H at 120ºC for 10 hrs. The synthesised resin has much greater catalytic activity as that of sulfuric acid and other solid acids at comparable acid loading due to its substrate-adsorbing capacity and low activation energy.

- **Tian et al.**[51]**:** This literature depicts the synthesis of heteropolytungstate salts for preferential hydrolysis of MCC to reducing sugars in liquid phase. To remove the adsorbed water, Cs_2CO_3 was calcined at 450°C for 2 hours before usage. A titration approach was used to generate a range of acidic cesium salts with cesium concentrations ranging from 1 to 3. At room temperature, dropwise with a steady rate, sufficient quantities of a 0.10 mol/L Cs_2CO_3 aqueous solution were introduced to a 0.08 mol/L aqueous solution of $H_3PW_{12}O_{40}$. The solutions were gently heated at 50 °C to generate white solid powers after the ensuing milky suspensions were dried at room temperature overnight. This catalytic reaction was performed with agitation at 160°C for 6 hours (30 rpm) with 0.1g of MCC and 0.06mmol of the synthesized catalyst. The reaction was halted by quickly chilling the reactor with the help of an ice bath. The glucose yield was quite low (27%).

- **Chatterjee et al.**[52]**:-** In the presence of an ionic liquid 1-butyl-3-methylimidazolium chloride, our research group effectively used Amberlyst 36 an acidic heterogeneous catalyst to produce cellulose by hydrolyzing papaya peels. The hydrolysis process was place in a dedicated reactor with tungsten

halogen lighting. In that unique reactor, papaya peels are prepared (with ammonia solution) and hydrolyzed. The entire procedure was improved. 2.5 percent ammonia concentration, 20 percent ionic liquid concentration, and 7.5 percent Amberlyst 36 concentration were the best reaction conditions. The pretreatment temperature was 70°C, while the hydrolysis temperature was 80°C. The pretreatment and hydrolysis reaction times were chosen at 20 and 10 minutes, respectively. It was discovered that the highest decreasing sugar yield was 89.02%. The best-fitting mechanism was identified as the Eley Rideal model after a kinetics evaluation of both processes. In comparison to a non-radiation reactor, the specifically constructed quartz halogen lamp fitted reactor lowers the activation energy of the process.

- **Qi et al.**[53]**:-** In this study, ceramic membrane based porous polymeric solid acid catalyst was developed. The catalyst comprising poly (ionic liquid) as well as polysulfonic acid chains was used to catalyse the hydrolysis of raw wheat straw for the formation of glucose. The raw wheat straw have been pretreated with either acid (H_2SO_4) or alkali (NaOH) at a temperature of 121ºC for a duration of 1hr. The pretreated wheat straw was hydrolyzed using the prepared catalyst and using organic solvent ([EMIM]Cl and GVL) and water. At the optimum condition of 150ºC, 60 min and 10g of solvent (weight ratio of [EMIM]Cl: GVL: H_2O was 7.6: 1.9: 0.5) with 8 wt% wheat straw, a glucose output of 50.7% was obtained. 83.4% of cellulose and 90.5% of xylan were hydrolyzed to soluble sugars & furans under the above mentioned reaction conditions. The use of high temperature in both pretreatment and reaction as well as use of organic solvents makes the process less economic.

- **Shen et al.**[54]**:** This literature focuses on the hydrolysis of commercially available cellulose using a carbonaceous solid acid catalyst in a one-pot synthesis. Sucralose and p-toluenesulfonic acid were combined to create the solid acid catalyst. The catalytic site was given by the sulphonic group in toluenesulphonic acid, while the binding site was provided by the chloride group in sucralose. Ionic liquid 1-Butyl-3-methylimidazolium chloride was also utilised in a typical batch process. Aside from the reaction technique, the influence of several factors such as time, temperature, catalyst concentration, and water to ionic liquid ratio was investigated. The optimised conditions resulted in a TRS content of 67.6%. The process takes 1 hour and the temperature is 130°C.

- **Shrotri et al.**[55]**:** This research looked at the depolymerization of cellulose using various solid acid catalysts. Eucalyptus timber was used to produce cellulose. In this study, cellulose was transformed into glucose and sorbitol. The hydrolysis of cellulose resulted in the production of glucose. Sorbitol was created by hydrolyzing cellulose and then hydrogenating it. In the procedure, heterogeneous catalysts were used. Within sorbitol synthesis process, metallic catalyst & hydrogen gas were supplied. The optimum parameters were able to obtain a sorbitol content of 99 %, however greater reaction conditions were required. In contrast, a solid acid catalyst was utilised throughout the hydrolysis phase to create glucose, yielding 90% sugar. The reaction time is 20 minutes. Another difficulty encountered during this procedure is that the glucose generated easily dissociates in hot water.

- **Jin et al.**[56]**:** This paper investigates the acid catalysed hydrolysis of microcrystalline cellulose into glucose. Amberlyst-15 catalyst, which is commercially available, was changed by combining it with a chloromethyl group. This newly manufactured catalyst has a larger surface area than the A-15 catalyst. The catalyst's sulphonic ion assisted in breaking the β-1, 4 glycosidic link, increasing the pace of the hydrolysis process. The chloride ion, on the other hand, formed hydrogen bonds with the cellulose molecules. The catalyst's successful operation was attributed to the two combining actions of anions in it. This technique yielded a maximum glucose output of 67.2%. The reaction temperature and duration were recorded as 170°C and 120mins, respectively. Another advantage of employing this specific catalyst is that the catalyst may be readily separated from the reaction stream using a sieve. The same catalyst is effective for up to five reuses.
- **Qu et al.**[57]**:** The development of a bifunctional recoverable catalyst for the hydrolysis of cellulose into fermentable sugar was reported in this literature. A silver doped phosphotungstic acid catalyst was developed to aid in the hydrolysis of microcrystalline cellulose in conjunction with an ionic liquid of 1-butyl-3-methylimidazolium chloride. As a result, the produced catalyst has both a binding site and a catalytic side for hydrolysis reaction. The hydrolysis process with cellulose was carried out in a round bottom flask. The ionic liquid ratio is set at 4:1. Concentration of catalyst, reaction temperature, and reaction time were the three parameters optimized to provide the maximum glucose conversion and yield. According to the literature, an ideal TRS yield of 71.8% and cellulose conversion of 100% for a temperature of 140 °C and a time of 1.5 hours. It was also noted that as the duration exceeds 1.5 hours, the conversion

rate reduces dramatically. The same process was carried out in three additional solvents than ionic liquid, namely water, DMSO, and THF, however the greatest conversion was only recorded in ionic liquid. Centrifugation successfully recovers the catalyst after the reaction. At the fifth cycle, the catalyst yields a conversion of up to 65%.

3.2 Pre-treatment of Lignocellulosic Biomass

Carbohydrate polymers (cellulose, hemicellulose) as well as an aromatic polymer ((lignin) make up the lignocellulosic biomass. Different sugar monomers (C6 and C5) are firmly linked to the lignin in these carbohydrate polymers. Because cellulose is the major feedstock for biofuel or platform chemical production, one of the processes for increasing the yield is to isolate the cellulose in the biomass by delignification. This separated lignin can be further used as bitumen modifier for sustainable roads[58]. Several pretreatment methods to delignify the LB have been developed including mechanical, chemical and other processes. In several published article we also find that biomasses are not delignified and is directly converted to valuable chemicals. In either cases the feedstock is first cleaned and dried then milled/cut/grounded to achieve a particular size range for further processing.

- **Zhao et al.**[59]**:** Cassava was processed with a combination of ethanol and aqueous H_2SO_4 because it contains 75.50 percent starch, 12.23 percent cellulose, 6.41 percent hemicellulose, and 4.58 percent lignin. When the ethanol to water ratio is 4:1, the cassava is efficiently depolymerized, with 78.53 percent cellulose and 8.89 percent lignin in the depolymerized residue, according to compositional analysis. However when cassava was treated with low ethanol to

water ratio (1:4) the residue mainly composed of lignin (76.15%) and cellulose content was 14.32% which is slightly greater than the cellulose content of cassava (12.23%). As an outcome, the solvent has a beneficial influence on cassava delignification, which promotes the carbohydrate's swelling and depolymerization, resulting in efficient LA formation

- **Chin et. al.**[60]**:** In this study the EFB fibers were first pretreated in ball mills to decrease the size and the crystallinity of the fibers. The size and crystallinity of the raw fibers were 125-500µm and 57.16% respectively which reduced to 80 – 106 µm (size) and 49.49% (crystallinity) after ball milling for 12 h and further decreased to <60µm (size) and 42.83% (crystallinity) after ball milling for 24 h. Ball milling (BM) alters the physical structure of fibers by decreasing hydrogen connections between cellulose, hemicellulose, and lignin, allowing cellulose to become more accessible [61]. However after reaction time of 180 min in the temperature range of 160 – 200°C the effect of BM pretreatment reached a plateau. The effect of BM was also less significant at 200°C. As a result, the energy required to break the crystallinity domains of EFB fibers prior to the acid hydrolysis process producing LA is not substantial for longer reaction times and higher reaction temperatures.
- **Daiane et al.**[15]**:** Rice Husk is known to have high lignin (25% - 30%) and silica (15% - 20%) percentage hence pretreatment of rice husk is very important. Several pretreatment methods have been examined and compared for product yield by Daiane and co-workers. They found that aqueous extraction using Soxhlet extraction gave the highest yield. Neither pretreatment with oxalic acid nor H_2O_2 in alkaline medium had any visible advantage. Organic solvent

(Benzene – ethanol 1:1) Soxhlet extraction and chlorite gave higher yield than oxalic acid and H_2O_2 in alkaline medium but lower than aqueous Soxhlet extraction.

- **Thakkar et al.**[62]**:** It has been reported in this study that hydrothermally treating the corn stover using K2CO3 decreased the lignin and hemicellulose percent from 27% to 18% and 21.6% to 8.7% respectively thereby increasing the glucan (cellulose) content from 28.2% to 62%. Thus K_2CO_3 successfully extracted 76% of lignin and 85% of xylan while preserving 83% of glucan. 11g of milled corn stover was firstly packed in a reactor. Dependent on the range of temperature, the experiment was separated into three 20-minute phases: heating (25–190ºC) followed by reaction (190ºC) & then cooling (190–50ºC). Using the high-pressure pump, a 0.45 wt percent K_2CO_3 solution was pushed into the reactor. Flow rates of 2.5 ml/min were maintained during the heating and reaction phases, while 9.9 ml/min were maintained during the cooling phase. A constant pressure of 3.44 Mpa was applied to maintain the liquid phase of water. The solid fraction was separated from the liquid and used in further reaction.

- **Pielhop et al.**[63]**:** The impact of explosive decompression in the steam explosion treatment of spruce wood pellets on enzymatic cellulose digestibility was thoroughly investigated. Steam at 32 bar was supplied to the reactor. To decrease steam condensation during experiment and the time necessary to get the metal reactor to the proper temperature, the reactor was first pre-heated by leaving it to remain filled with steam of the desired study temperature (210ºC) for 10 minutes before every experiment. The steam & condensate were

discharged once more, as well as the reactor was promptly repressurized to 19 bar and filled with 1.5 kg of new spruce wood chips. The wood chips were treated for 10 mins and the pretreated wood chips were used for further study. When contrasted to a steam pretreatment with no explosion, the explosion had a significant impact on digestibility, enhancing it by up to 90%.

- **Teymouri et al.**[64]**:** In this study corn stover has been treated by ammonia freeze explosion experiment (AFEX) method. Corn stover were soaked with distilled water to a moisture content of 60 % (dry basis) and left to reach equilibrium for 30 minutes before being treated with AFEX. In the pressure vessel, the pre-wetted samples were deposited. The jar was then filled with stainless steel pellets (about 1mm diameter) to fill the blank area and prevent the ammonia from converting into gas during loading. The lid was then fastened shut. To charge the system, pre-calibrated sample cylinders had been filled with the required amount of ammonia (1kg/kg of feed). To warm the unit to a temperature of 90ºC, the complete reactor assembly was put in a heating mantle. Following the completion of the experiment, the exhaust valve was quickly opened to alleviate the pressure and finish the explosion. The treated corn stover was removed and left in a fume hood overnight to evaporate any remaining ammonia. The findings of enzymatic hydrolysis of AFEX-treated corn stover revealed that the pretreatment is successful.

- **MacDonald et al.**[65]**:** Corn stover was treated with alkaline solution in this research. The reactor has been loaded by filling the vessel with 15.9 g of corn stover & 225 mL of distilled water and 25 mL of NaOH solution. After that,

the vessel was shut, the stirrer was adjusted to 200 rpm, and steam was pumped through coil at maximum line pressure to meet maximum heating rate (1 minute to reach 100°C, 2 minutes to reach 150°C). The stirrer speed was then increased to 700 rpm when the steam pressure was decreased to the point at which temperature in the reactor remained constant. The steam was shut off and cooling water was fed through the coil once the reaction time was reached. Filtration was used to separate the particulates from the liquid once the reactor's contents were evacuated. To determine the quantity of sugar available, the solids was dried, weighed and processed enzymatically.

- **Mosier et al.**[66]**:** This review stated that H_2O_2 can be used as an oxidising agent can to deignify biomass. Lignin and hemicellulose are removed from lignocellulose to a greater level in this method. Oxidizing chemicals react aggressively with the aromatic rings of lignin in this procedure, resulting in aromatic carboxylic acids that might function as inhibitors in subsequent stages of transformations, therefore they must be eliminated or neutralised before processing the celluloses.

- **Chen et al.**[67]**:** This study generated cellulose compounds from red algae, a marine biomass. As per the author, marine biomass has very little or no physical or chemical barrier, thus no significant pre-treatment is necessary to make cellulose molecules more accessible. Algal biomass also grows quickly, allowing it to fulfil the growing need for feedstock. According to studies, sea red algae such as Gelidium elegans retain a high carbohydrate concentration that may be efficiently converted to galactose and glucose. The raw algal biomass

included 19.1% cellulose, of which this study was able to extract more than 90%. At 80 degrees Celsius, the biomass had first been treated with a dilute NaOH solution. The resultant mass was then bleached with 30 percent H_2O_2 before being acid hydrolyzed with 64 weight percent sulphuric acid. The alkalization procedure proved successful in removing hemicellulose, and bleaching virtually totally removed the lignin component (upto 99.3%). The final nano-cellulose produced had 90.8 percent cellulose, 1.3 percent hemicellulose, and a minimal amount of lignin (< 0.5%). This project's main goal was to produce high-purity cellulose. Although the method is hazardous per life cycle assessment due to the use of caustic sulphuric acid (64 wt.%).

- **Rahman et al.**[68]:- Leftover tea leaves were employed as a feedstock in this study to synthesise nanocrystal cellulose particles. The tea fibers were first treated with a 4 wt.% NaOH solution. The alkylation was carried out in an 80°C mechanically stirred reactor. It was then bleached for 4 hours at the same temperature using aqueous sodium chlorite solution and glacial acetic acid solution. The next phase was hydrolysis using sulphuric acid. The hydrolysis was performed at 45°C for 45 minutes. Following the reaction, the fibers were extracted from reaction mixture using a 9500 rpm centrifuge. The discarded tea leaves feedstock included roughly 16.2 % cellulose, with an 87.9 % conversion rate.
- **Wang et al.**[69]**:** This literature has made use of discarded cotton cloths to extract cellulose and then convert it into nano crystals of cellulose. The cotton cloth's cellulose content was determined to be substantially high, at 90%. Instead of dumping or incinerating the cotton cloths, they were utilised to extract cellulose.

Because it is a trash, the price of feedstock is likewise very low. This project concentrated just on recycling of discarded cotton textiles. To maximise efficiency, this method used combined acid hydrolysis (HCL 37wt.% and H_2SO_4 98wt.%), with a conversion rate of 87.9%. Both H_2SO_4 and HCL have benefits. Because it is a powerful acid, sulphuric acid accomplishes the hydrolysis reaction with significantly greater efficiency. The sulphate anion plus H+ cation rapidly dissolve, accelerating ion exchange. Hydrochloric acid, on the other hand, regulates the oxidation process. As a result, the combined acid had a high conversion rate. First, the discarded cotton cloths were transformed into pulp. The pulps were then steeped in the combined acid concentration. The ratio of Deionized water to H_2SO_4 to HCL is held at 11:3:1, followed by 7 hours of ultrasonication. Additionally, centrifugation at 10,000 rpm & freeze death at -60 ° C were performed. The findings indicated that cellulose nanocrystals generated from pulp have a significant crystallinity index (55.76 %).

Chapter 4

AIMS & OBJECTIVES

4.1 Aims and Objective

1. Synthesize reducing sugar from an agricultural waste (Corncob).

2. In addition, a cost-effective E-waste-derived catalyst combining the effects of photo-catalysis & acid-catalysis would be developed.

3. The use of anti-ionizing Quartz-Halogen radiation inside the reactor for hydrolysis of corncob fiber has to be investigated and verified as an effective energy source for a possibly greater output of reducing sugar than a conventionally powered reactor.

4. A comparison of energy consumption between a traditionally heated reactor (THR) or an unconventionally (radiation) heated reactor will be conducted (QHSR).

5. The cost of the overall process will estimated and compared to commercial catalyst.

6. Another element of this project will be a life cycle environmental impact assessment, which will use OpenLCA software to examine the environmental impact (if any) of the aforementioned procedure.

Chapter 5

MATERIALS

5.1 Materials

- Wasted Printed Circuit Boards (W-PCB) were collected from regional scrap stores in Kolkata
- Corncob has been collected from local vendors in Kolkata.
- Deionized (DI) water, distilled water and tap water.
- Ammonia solution (90%).
- Acetone.
- Hydrogen Peroxide (H_2O_2) (50%).
- Glacial Acetic Acid (>99%).
- N,N-Dimethylformamide (DMF).
- Sodium Hydroxide pellets.
- Gallium (III) nitrate hydrate.
- Bis(acetylacetonate) dioxomolybdenum (VI).
- Sulphuric acid (H_2SO_4).
- Potassium sodium tartrate.
- 3,5-dinitrosalicylic acid.
- Phenol.
- Sodium sulphite.

*all the chemicals of analytical grade was bought from Sigma Aldrich.

Chapter 6

METHODS

6.1 Glass fiber support preparation

All unnecessary elements, such as conductive rails and RAM, were disassembled and physically removed from the W-PCB. The W-PCB was then cut into pieces of 5cm x 5cm and the pieces were then immersed in 10 M NaOH for 24 hours without agitation before being washed in water[70]. As a result, the metal alloys were delaminated from the surface and the surface coating was removed, revealing the copper clad. The W-PCBs were then ground in an ultrafine grinder, i.e. a drum sander, passed through an ASTM 45 mesh (~ 355µm). The ferrous elements in W-PCB were then removed by employing a wet magnetic stirrer (100 W) for 0.5 h. Sedimentation partly eliminated the remaining heavy particles such as tin, aluminum, zinc, and lead. After that, the resulting combination of glass fiber, copper, and other materials was washed and collected by filtering. After that, DMF (Di-Methyl Formamide) was applied to that same powder to eliminate the epoxy resin. Following that, copper was totally removed by agitating the sample with 1 M acetic acid and 5 ml of H_2O_2 (30% w/w in H2O) solution for 2 hours. The glass fiber was carefully cleaned and collected after the copper was extracted as copper acetate. The extracted glass fiber (GF) was then treated with an ultrasonicator (250W) for 45 minutes to reduce its size before being recovered by filtering. Finally, the GF was dried in a hot air oven at 105 °C and employed as a catalyst preparation support.

6.2 GaMo-GF catalyst preparation

By changing the gallium precursor loading (2, 4, 6 wt. % percent of GF) with a given quantity of molybdenum, three gallium-molybdenum catalysts have been prepared. The catalyst was made utilizing the wet impregnation process. 0.36g of gallium (III) nitrate hydrate, 0.34g of Bis (acetylacetonate) dioxomolybdenum (VI), and 5g of GF were

placed in 70ml acetone and agitated for 10 minutes under moderate heating to make a 4 wt. % catalyst. After 10 minutes, 2 mL ammonium hydroxide was added, and the mixture was agitated for another 40 minutes under gentle heat. The mixture was allowed overnight before being ultra-sonicated for 30 minutes to produce nano-impregnation. The mixture was then filtered, and the residue was oven dried at 80 °C for 24 hours. The oven-dried powder was then calcined for 2 hours at 700 °C. The calcination temperature was determined through TGA analysis of the sample.

6.3 Pretreatment of Corncob

The procured corncob was carefully cleaned with hot water and dried. It was then grounded to produce uniformly fine particles (-250 ~ +300 mesh screen). Following that, corn cob was delignified using the method described by Watkins et al[71]. To separate lignin, 40g corn cob was heated for 3 hours at 80 °C with a 100 ml acetic acid plus H_2O_2 mix solution (9: 1) solution. The resultant mixture was then filtered and the residue was collected. The residue was then washed with hot water and ultra-sonicated for 30mins. It was then filtered and the residue was dried overnight in a hot air oven at 60ºC. The DCC was then used for experimental runs.

6.4 Compositional Analysis of Corncob

The composition of the corncob and DCC was analyzed for cellulose, hemicellulose and lignin content. The lignin content was measured by measuring the weight difference of the corncob before and after the treatment with peroxide acetic acid. The cellulose and hemicellulose content was calculated by completely hydrolyzing the corncob with conc. H_2SO_4 and measuring the glucose (for cellulose) and xylose (for hemicellulose) content in the hydrolysate by using HPLC analysis. The method was repeated for the compositional analysis of DCC. The compositional analysis of corncob and DCC are

presented in Table S1. Furthermore, the DCC's carbon, hydrogen, nitrogen and sulphur content has been analyzed using CHNS analyzer, and the results are given in Table 4.

6.5 Preparation of DNS for yield calculation of RS

To prepare DNS solution as per the process described in Miller et al.[72], 125mL of deionized (DI) water is taken and gradually 45.5g of potassium sodium tartrate, 1.6g 3,5-dinitrosalicylic acid and 65.5mL 2N NaOH is added with it. The solution is then heated to 50 ° C in a conventional water bath heater. After heating, 1.25g phenol and 1.25g sodium sulphite is mixed with it and stirred until uniform homogeneity is achieved. Next, the solution is cooled down to room temperature and 250mL of DI water is added for dilution to obtain the final DNS solution.

6.6 Process optimization using Taguchi's Design

To optimize the hydrolytic degradation reaction parameters, Taguchi Orthogonal Array design (TgOD) is employed. A Taguchi experimental design is created in Minitab software. 4 independent parameters are given as input. A 3 level 4 factorial design is created which required to take 9 experimental runs to give the optimised results. Signal to noise ratio is calculated

6.7 Estimation of reducing sugar

The reducing sugar yield has been determined using UV-Vis Spectroscopy. Firstly dinitrosalicylic acid or DNS was prepared using the method described in Miller et al.[72]. A combination of 1ml of DNS solution, 1ml of the hydrolysate was combined in a test tube subsequently heated at 90°C in a typical water bath heater to measure the TRS yield achieved from the photo-hydrolysis reaction. The solution was cooled to room temperature after 5 minutes of heating. It was then diluted with 9 ml of DI water using a 10 dilution factor. This mixture was examined in UV spectrophotometer. A

calibration curve of absorbance vs concentration of glucose at a wavelength of 540nm was prepared beforehand (Figure 9). The resultant absorbance of the hydrolysate was used to find the respective RS concentration.

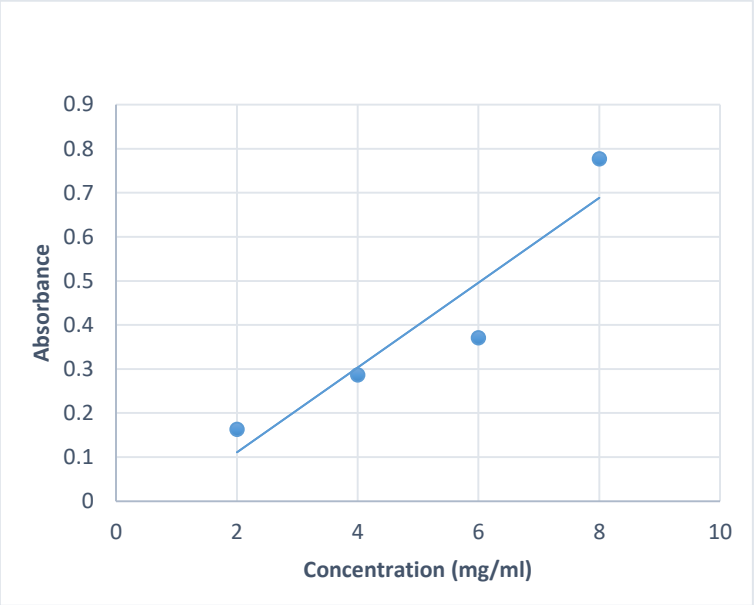

Figure 9: Standard glucose calibration curve at 540nm

6.8 Photocatalytic hydrolysis of corncob

Photocatalytic degradation of the delignified corn cob was performed in a quartz–halogen solar batch reactor (QHSR). 250 mg of delignified corn cob was measured and added to 20 ml of distilled water in a single necked round bottom flask (50 ml) equipped with a centrally fitted stirrer. A specified quantity of prepared photocatalyst was added to afore mentioned mixture. The reaction mix was stored in the dark condition at 25 °C for 20 minutes before the photocatalytic reaction to achieve adsorption equilibrium. Thereafter the radiation was applied and the mixture was rotated at 850 rpm. A PID controller was used to keep the temperature stable. 4 independent control parameters, namely reaction temperature (R_T), time (R_t), catalyst concentration (C_c), and gallium precursor loading (P_L), were used to monitor photo-degradation [Table 2].

Table 2: Degradation of delignified corncob in QHSR with independent process parameters.				
Factors	Units	L_{-1} Level	L_0 Level	L_1 Level
Reaction Temp. (R_T)	ºC	70	80	90
Gallium precursor loading (P_L)	weight %	2	4	6
Catalyst Concentration (C_c)	weight %	5	10	15
Reaction time (R_t)	minutes	20	30	40

Through nine experimental runs using L9 TgOD (Minitab Inc. USA for Windows 10) [Table 2], the impacts of four process parameters on the cellulose degrading process were analyzed and adjusted. The best process variables corresponding to maximal RS yield (Y_{RS}) were identified using the "bigger is better" criteria to evaluate signal-to-noise (S/N) ratios (Eq. 2) and analysis of variance (ANOVA).

$$\frac{S}{N} = -10 \log\left(\frac{1}{n}\sum_{m-1}^{n} 1/\,Y_{TRS,m}{}^{2}\right) \qquad \text{(Eq. 2)}$$

where, n represents the number of experiments done at a specific set parameters [Table 3], m reflects the amount of repetitions, and Y_{RS},m is the Y_{RS} relating to run n.

Table 3: TgOD diagram for the GaMo-GF catalyst used for the photocatalytic hydrolysis of delignified corn cob.					
Experimental Run	R_T (ºC)	R_t (min)	C_c (wt %)	P_L (wt %)	RS yield (mol %)
1	80	20	5	2	25.12
2	80	30	10	4	45.16
3	80	40	15	6	51.93

4	90	20	10	6	56.24
5	90	30	15	2	63.39
6	90	40	5	4	53.91
7	100	20	15	4	72.47
8	100	30	5	6	53.31
9	100	40	10	2	52.43

6.9 Life-cycle Analysis

A relative environmental impact assessment evaluation was carried using OpenLCA 1.11.0 software to determine the viability of the improved process design for use of QHSR over thermally heated reactor (THR) in the production of RS by catalytic hydrolysis of DCC. Additionally, the possible effects on the environment for the preparation of the W-PCB derived GF supported Ga-Mo catalyst has also been assessed. The ISO Standard 14,040:2006[73] has been followed in the implementation of life-cycle assessment (LCA). Climate change (GWE100), fossil depletion (FSD), ionising radiation (IR HE), human toxicity (HTL), metal depletion (MeDP) and water depletion (WaDP) are the environmental indicators examined in this study. The GWE100 represents the comparable quantity of CO_2 released by the process. It is expressed in kilos of CO_2 equivalent.

The whole process flow and system boundaries for LCA are depicted in a schematic Figure (Figure 10). The system has been divided into three boundaries. The 1st system boundary includes the extraction of GF from W-PCB and the preparation of the GaMo-GF catalyst. Here, life cycle inventory results were evaluated based on the manufacturing of 1 kg GaMo-GF (4 wt. %) photocatalyst. The 2nd system boundary

comprises of the processing & delignification of the corncob, in which, life cycle inventory results were evaluated based on the manufacturing of 1 kg of DCC. Finally the 3rd system boundary incorporates the photocatalytic hydrolysis process where the life cycle inventory results were evaluated based on the manufacturing of 1kg of RS. The study findings have been up-scaled as per the functional units and provided as a database for said Life Cycle Inventory (LCI).

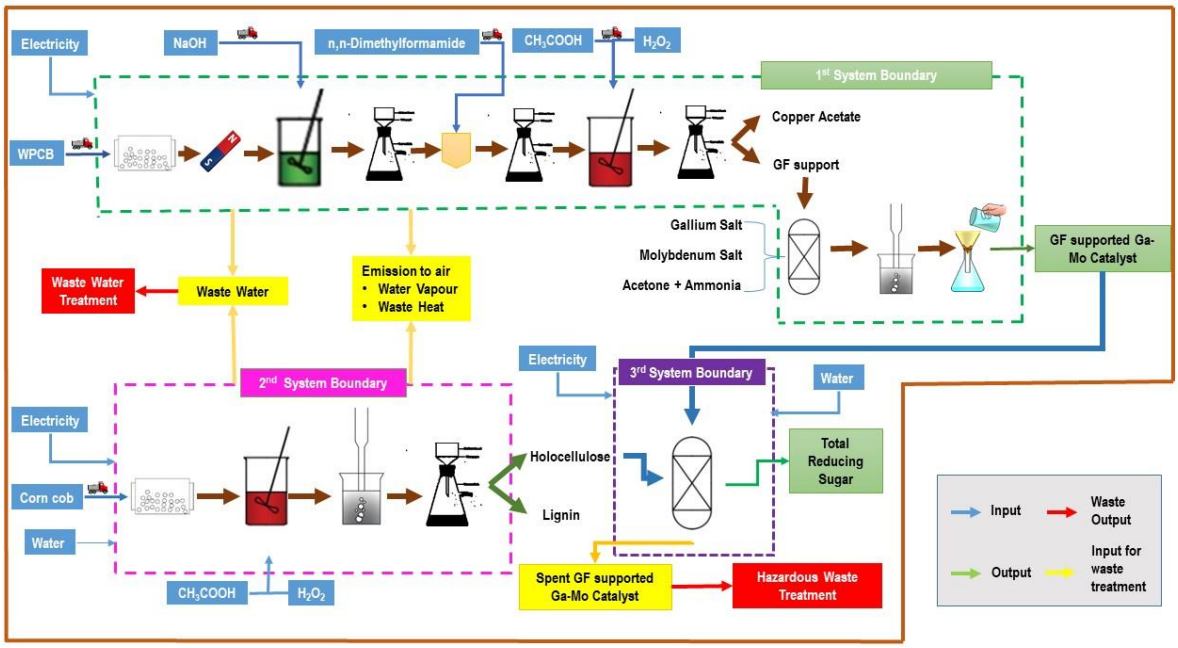

Figure 10: System boundaries and process flow diagram for LCA

6.10 Goal and Scope of LCA study

The scope of a procedure defines its boundary. Among the two basic types of borders, the cradle to gate method is responsible for only calculating impacts that occur within the boundary. The study's goal is to identify hotspots, which identify the specific process responsible for the greatest amount of GWE100 emissions. Other environmental effect factors such as FSD, IR HE, and HTL are also assessed. The

research focuses on three important processes in RS synthesis: pre-treatment, delignification, and PH reaction (Figure 10). The current sustainability study solely considers environmental effect. Furthermore, this work excludes the treatment & discharge of waste effluent streams.

6.11 Characterization of the synthesized catalyst

Characterization of the optimum GaMo-GF catalyst was done (on basis of the highest RS yield according to TgOD). Utilizing Cu Kα radiation with a wavelength of 1.5147 Å, X-ray diffraction (XRD) patterns of the GF support and the prepared catalyst were obtained on a Bruker D8 Advance diffractometer. TGA study was performed out in a PerkinElmer, Pyris Diamond TG/DTA analyzer with N_2 flow (1.2L/h) at a heating rate of 10.0°C/min from 25ºC to 780ºC. The GaMo-GF's infrared spectra were also discovered using an FTIR-Shimadzu (Alpha) instrument with a wavelength range of 400 to 4500 cm^{-1}. BET analysis on a NOVA touch 2LX was used to estimate the surface area as well as pore volume of the manufactured optimum catalyst. The specimen was firstly degassed at 250°C in order to remove moisture from the surface. FESEM (JSM-6360 (JEOL Ltd.) at 15 kV and HRTEM were also used to investigate the surface morphology of the GaMo-GF catalyst. Elemental analysis and mapping were performed on Bruker's XFlash® 6 detector series using EDAX analysis. X-ray photoelectron spectroscopy (XPS) of the GaMo-GF was used to measure the binding energy as well as oxidation state of various elements contained in the catalyst specimen. The samples acidity were determined by NH_3-TPD analysis (Quantachrome Instruments), TPR win v2. The photocatalytic characteristics of optimum GaMo-GF catalysts was investigated using a Perkin Elmer LAMBDA 950 UV-VIS-NIR Spectrophotometer with a tungsten halogen lamp as the light source.

6.12 Analysis of hydrolysate

A Waters HPLC system with RI detector (Perkin Elmer 200 series) was used for the chromatographic separation of reducing sugars (glucose and xylose). The mobile phase was acetonitrile & water (60:40, v/v), with a flow rate of 1 ml/min. The injection volume was 10µl. A Breeze Chromatographic System was used for peak detection and integration (Waters Company, Milford, MA, USA). After equilibrating the column with a mobile phase, the flow rate was maintained at 1.0 mL/min, and 10µL of standard solution subsequently injected into the chromatographic column. The calibration plots of the corresponding standard constituents were used to calculate the concentrations of the hydrolysate constituents. At the completion of each experiment, the column was rinsed with said mobile phase for more than 30 minutes.

Chapter 7

RESULTS AND DISCUSSION

7.1 Chemical composition evaluation of corncob and DCC

The composition of corncob and DCC was determined in order to determine the samples' holocellulose and lignin contents and the results are depicted in Table 4. Its surface contaminants and the bulk of the lignin fraction were removed by the hydrogen peroxide and acetic acid treatment as is evident from the decrease in lignin content from 17.3% to 2.1%. Some of the hemicellulose portion was also eradicated by the treatment process. The CHNS analysis of the DCC is presented in Table 5.

Table 4: Composition of corncob and DCC

Biomass	**Cellulose (wt. %)**	**Hemicellulose (wt. %)**	**Lignin (wt. %)**
Corncob	33.54	32.16	17.3
DCC	75.14	22.65	2.1

Table 5: CHNS analysis of DCC

Carbon (%)	**Hydrogen (%)**	**Nitrogen (%)**	**Sulphur (%)**
43.30	5.686	0.39	0.219

7.2 Photocatalytic hydrolysis of DCC under optimal conditions.

Table 6 displays the rankings of four process parameters acquired from the experimental designs and the L-9 TOD projected values. The value of delta (δ) determines the rank; the greater the value of δ, the higher the rank. The process variable with the greatest effect on the reaction is determined by rank. It can be seen from the table that the reaction temperature (R_T) plays the most significant role in the photo hydrolysis of corn cob closely followed by the catalyst concentration (C_c). Furthermore, ANOVA analysis [Table 7] for the photocatalytic corncob hydrolysis process

confirmed R_T and C_c were statistically important process parameters at the 95% confidence level (p-value < 0.05). On the other hand the highest Signal to Noise ratio (S/N) values indicates the process factor's optimum level. Accordingly from Table 4 it can be deduced that L_{+1} of C_C (15 wt. %), L_0 of P_L (4 wt. %) were the optimum process values. The S/N ratio of R_T at 100ºC is the highest hence L_1 of R_T (100ºC) is identified as the optimum reaction temperature although the yield only increases slightly. Similarly for reaction time L_0 is identified as the optimum R_t (30 min).

Table 6: S/N ratio and delta values for GaMo-GF catalysed photo hydrolysis of corncob

Level	**Temperature**	**Time**	**Catalyst Concentration**	**Precursor Loading**
L_{-1}	31.80	33.40	32.39	32.81
L_0	35.22	34.56*	34.16	34.98*
L_{+1}	35.38*	34.44	35.85*	34.62
Delta (δ)	3.55	1.20	3.31	1.88
Rank	1	4	2	3

Table 7: ANOVA table of process parameters

Term	**Coef**	**SE Coef**	**T-Value**	**P-Value**	**VIF**
Constant	-58.9	30.7	-1.92	0.127	
R_T	0.933	0.309	3.02	0.039	1.00
R_t	0.074	0.309	0.24	0.822	1.00
C_c	1.848	0.618	2.99	0.040	1.00
P_L	1.71	1.54	1.11	0.330	1.00

7.3 Reaction mechanism

The synthesized optimum GaMo-GF photo-catalyst significantly facilitated the DCC hydrolysis process. Being a photo-catalyst the GaMo-GF generates electron-hole pair when exposed to radiation (Figure 11). The generated hole reacts with water to form H^+ ions and hydroxyl free radicals. The generated H^+ ions forms a hydronium ion with another water molecule (the H^+ could direct attack the holocellulose as well but since water is a better proton acceptor the formation of hydronium is more probable)[74]. The hydrogen and the β-(1→4) glycosidic linkages in the DCC are attacked by the generated H_3O^+ ions to form β-(1→4) glucan; which is then hydrolyzed to form glucose. Similarly, the β-(1→4) linkages in the hemicellulose of DCC are broken down to yield-reducing sugars.

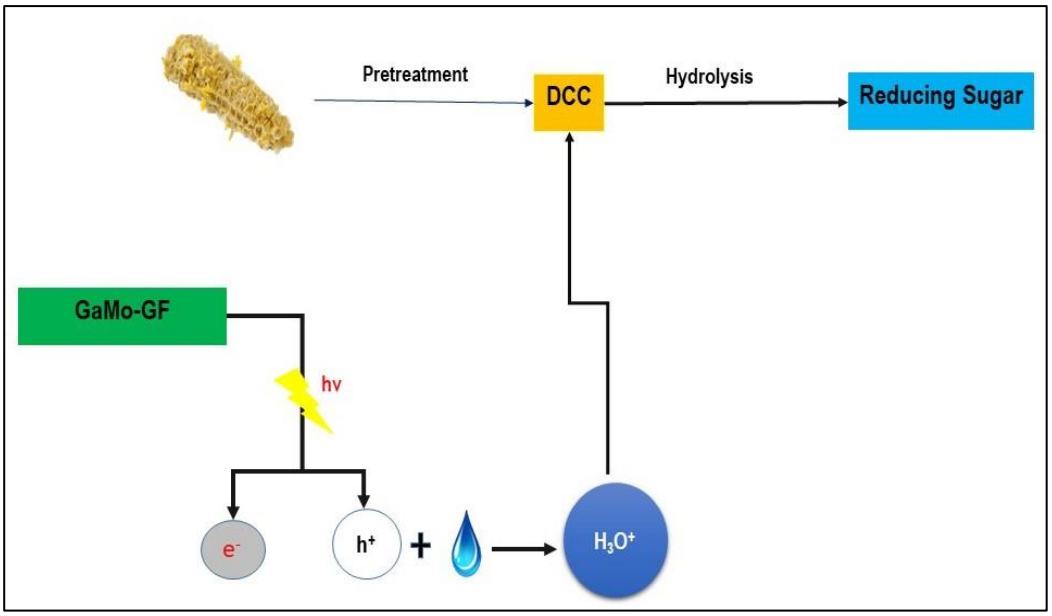

Figure 11: The photocatalytic hydrolysis reaction mechanism

7.4 Individual as well as interactive impacts of process factors on DCC hydrolysis

Figure 12(a) depicts the parametric interaction in the corncob hydrolysis process. From the Figure it can be seen that on increasing the temperature from 80ºC to 90ºC (keeping other factors constant) the RS yield increases but on further increase in temperature the yield is almost constant. This may be due to the fact that at higher temperature the RS may degrade. Similarly for reaction time after 30 mins the product might further degrade. On increasing the precursor loading (P_L) from 2 wt.% to 4 wt.% the surface acidity and the photocatalytic effect increases hence the RS yield increases. But further increase in P_L has a negative impact on the RS yield. Above 4 wt.%, the enlarged nanoparticle size blocked the GF support's pore, reducing the catalyst's total surface area dramatically (BET and XRD analysis). Also as the catalyst concentration increases the yield increases linearly this is due to the fact that more surface area is available for the reaction.

The photocatalytic hydrolysis of DCC's process' parametric interactions are shown in Figure 12(b). From the interaction plot of catalyst concentration vs. temperature, it can be seen that while keeping all other parameters constant, with an increase in catalyst concentration at all temperatures the yield of RS increased. This exemplified how the created GaMo-GF catalyst significantly facilitated the DCC hydrolysis process. A similar pattern was seen for all reaction time levels. At the same time, the catalyst concentration vs. gallium precursor loading plot revealed that increasing the gallium loading at a low concentration increased the RS yield. In contrast, at higher catalyst concentration, the RS yield increases till the gallium loading is 4 wt. %. Then it decreases due to the decrease in surface area and creation of bigger nanoparticles during catalyst preparation with increased precursor loading. Moreover,

the temperature vs. time graph reveals that at high temperatures, the RS yield decreases as time increases because of the degradation of RS.

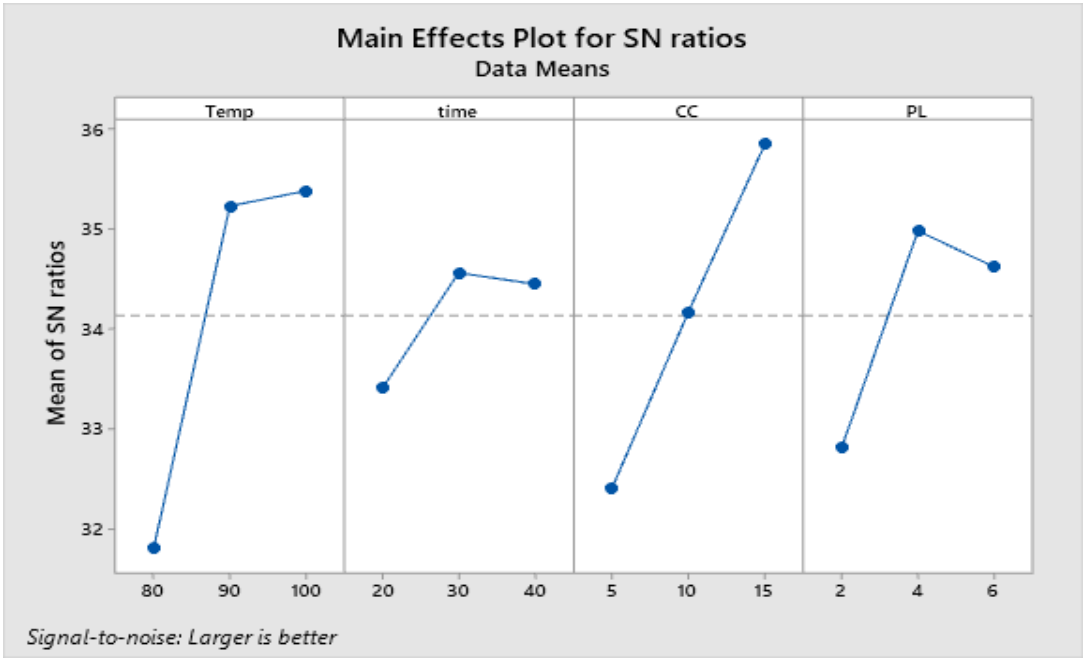

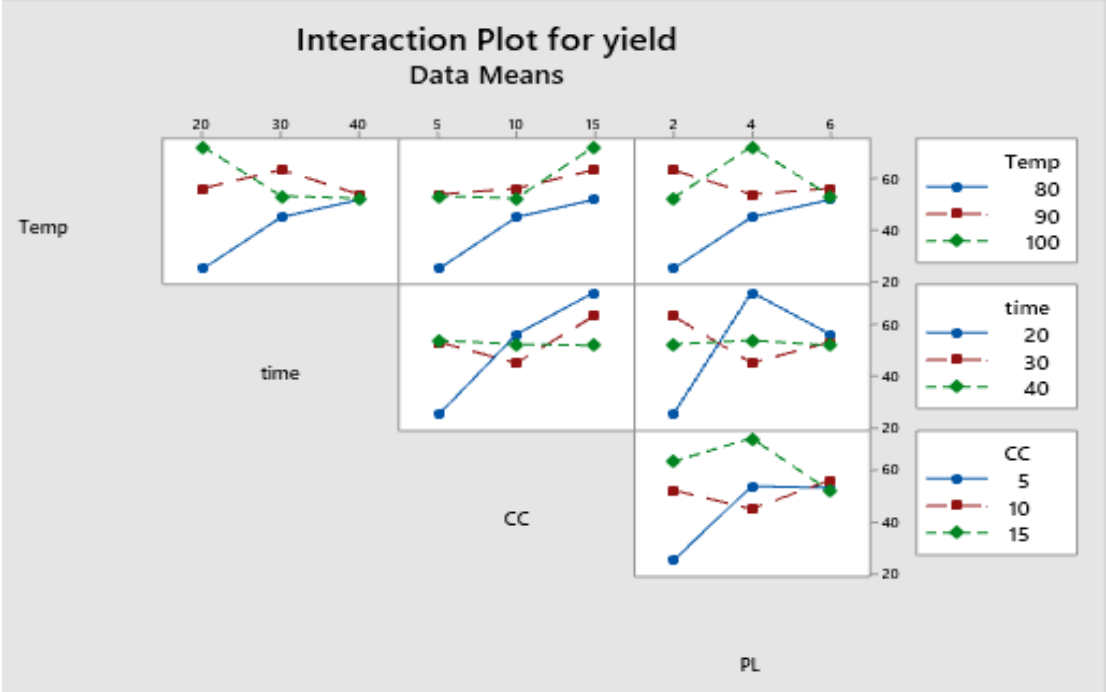

Figure 12: (a) Means of signal to noise ratio plot (b) interaction plot for RS yield

7.5 X-Ray Diffraction of GaMo-GF

The X-ray diffraction (XRD) patterns of Glass Fiber powder as well as calcined samples [GaMo-GF catalysts] are shown in the Figure 13. Peaks corresponding to the crystalline phase of molybdenum trioxide (33.15º, 49.48º, 55.22º) [75], gallium oxynitrate (26.62º, 47.04º, 58.04º) [76,77], β-gallium oxide (47.56º), silicon-oxide (22.8º) [78] and aluminum-silicon oxide (18.64º, 28.72º) [79] have been discovered in all catalysts as shown by plots A, B, C. The presence of silicon in the GF powder is demonstrated by the hump as shown in the Figure, which is attributable to the presence of SiO_2 across all catalysts[80]. It can be concluded from the Figure that as the gallium loading is increased the peak intensity of gallium oxynitrate also increases. The sample's crystallite size (D_c) was determined using the equation of Debye-Scherer's:

$$D_c = {}^{0.9\lambda}/_{\beta \cos \theta}$$

where,

λ is the X-ray beam's wavelength (λ=1.5406)

β is the intense peak's full width at half maximum (FWHM)

θ is the Braggs angle.

Using the above equation, the crystalline size of MoO_3, GaON, β-Ga_2O_3, SiO_2 and Al_2O_3-SiO_2 are 6.97, 20, 15.54, 5.53 and 28.61nm respectively.

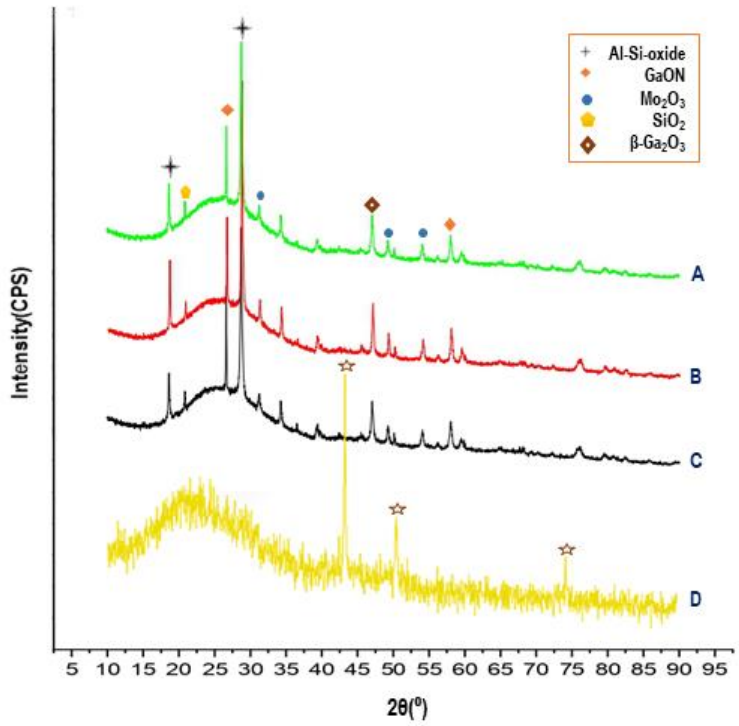

Figure 13: XRD of (A) 6 wt.% GaMo-GF (B) 4 wt.% GaMo-GF (C) 2 wt. % GaMo-GF (D) GF

7.5 Thermogravimetric Analysis (TGA)

TGA of GF and optimum GaMo-GF were carried out to establish the material's thermal stability when heated over a wide range of temperatures, ranging from 30 to 780 ºC, as shown in Figure 14. Since there was no weight loss after 650ºC, the TGA analysis was performed up to 780ºC. Over 270-370°C, the TGA thermogram of GF indicates a significant weight loss (31%), which is attributed to the degradation of un-extracted epoxy resin. The GF thermogram further reveals a weight loss of 15% from 400-650ºC; this was attributed to the oxidation of the solid residue generated during the first decomposition step[81]. The weight% vs. temperature graph of GaMo-GF shows a sharp weight loss of 10% in the temperature range of 110-200 ºC, evaporation of adsorbed water is most likely to be responsible for the occurrence of this behavior. Furthermore, from 200 ° C to 450 ° C, there is a progressive 13.5% weight loss due to the decomposition of gallium precursor salt to gallium oxides[82]. There is a further weight

loss of about 17% from 450°C to 650°C, which is due to the transformation of MoS_2 to MoO_3 and sulphur dioxide[83]. The generated catalyst was calcined in a muffle furnace for two hours at 700°C to solve this issue. As a result, the optimized GaMo-GF catalyst

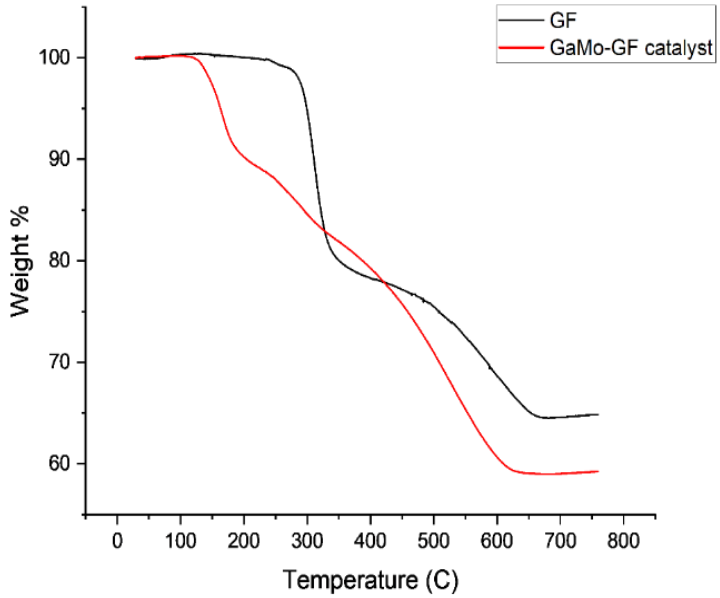

Figure 14: TGA of GF and GaMo-GF catalyst

demonstrated improved thermal stability. Since the photo-degradation of cellulose has been performed under 100°C (well below 650°C), the thermal degradation of catalysts was highly improbable.

7.6 Fourier transform infrared spectroscopy

The FTIR spectra of GF supported catalyst is depicted in the Figure 15. FTIR studies of the optimum catalyst revealed a peak at 3748.82 cm^{-1} owing to the existence of absorbed water with a significant OH stretching mode[84]. The broad peak at 2999.97 cm^{-1} and 2805.36 cm^{-1} corresponds to the C-H stretching vibrations[85]. Sharp peaks near 2274.42 cm^{-1} indicated the presence of C-N stretching modes in the produced catalysts[86]. The peak at 1508.2 cm^{-1} indicates the presence of nitro compound, which can be confirmed from XRD data to be GaON. Furthermore, the catalyst spectra

showed peaks at 764.22 cm^{-1} and 463.1 cm^{-1}, which relates to vibration of Ga-O[87]. The presence of Si-O [88] is evident from the peak at 1084.4 cm^{-1} and 811.24 cm^{-1}. Additionally, characteristic peaks at 996.52 cm^{-1} and 605.27 cm^{-1} might be ascribed to Mo-O bonds[88].

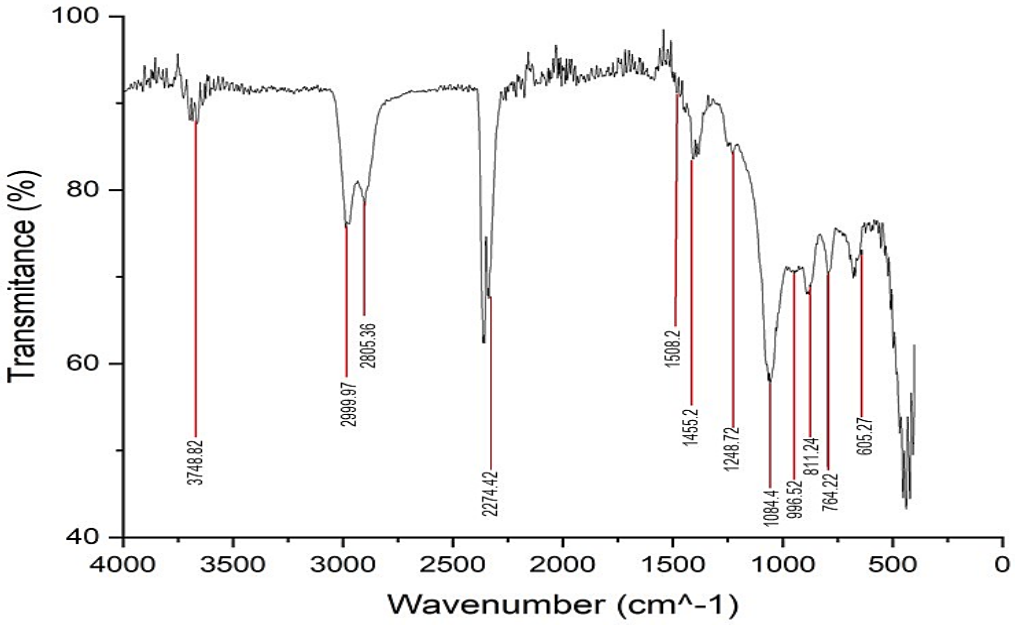

Figure 15: FTIR spectra of the optimum GaMo-GF catalyst

7.7 X-Ray Photoelectron Spectroscopy

XPS examination showed the electronic states of the component species of the optimal catalyst found using Taguchis's method. As illustrated in Figure. 16, Si 2p unfurls two peaks. The Si-O bond has been indicated by the binding energy of 103.5 eV. As noted in Figure 16, the first peak at 102 eV may be ascribed to the Al-O-Si Bridge (FTIR) of the GFR structure, which can be well supported by FTIR studies, and the binding energy of Al (=74.4eV) is a more credible sign of aluminosilicate presence. The two peaks at

233.4 eV and 236.2 eV, corresponding to Mo $3d_{5/2}$ and Mo $3d_{3/2}$ [89], respectively, in Figure 15, indicate that the Mo species is MoO_3. The peak of gallium at 19.97 eV and 24.01eV corresponds to the presence of GaON[90]. Finally the two peaks at 347.18 eV

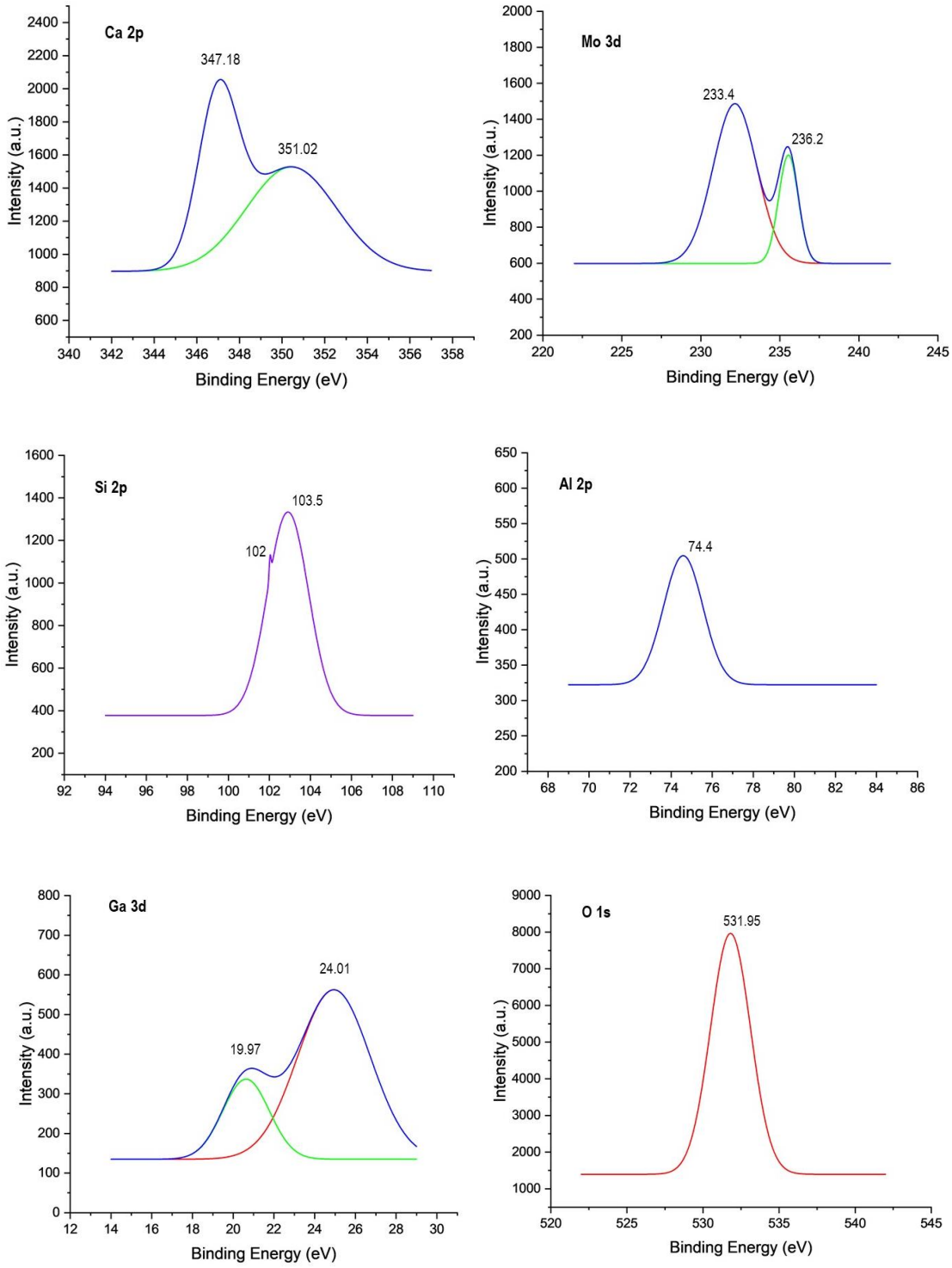

Figure 16: XPS of the optimum GaMo-GF catalyst

and 351.02 eV corresponds to Ca $2p_{3/2}$[91]. The occurrence of oxygen is also confirmed by a binding energy of O at 531.95eV in Fig 15 (XPSsimplified.com).

7.8 Scanning Electron Microscopy (FESEM) and EDAX

The surface morphology of the untreated W-PCB powder (Figure 17(a)), treated W-PCB (Figure 17(b)) and GF supported optimum GaMo-GF catalyst (Figure 17(c)) was revealed by FESEM analysis at various magnifications. The untreated W-PCB powder sample's morphology as seen in Figure 17(a) depicts fiber glass rods encased in epoxy resin in an uneven rod form. After treatment, the epoxy resin on the fiber glass rod was reduced and exposed the surface of the GF (Figure 17(b)) which in turn enhanced the surface area (revealed from BET analysis). Figure 17(c) depicts MoO_3 and GaON grafted GF support of the optimum GaMo-GF catalyst. Moreover,

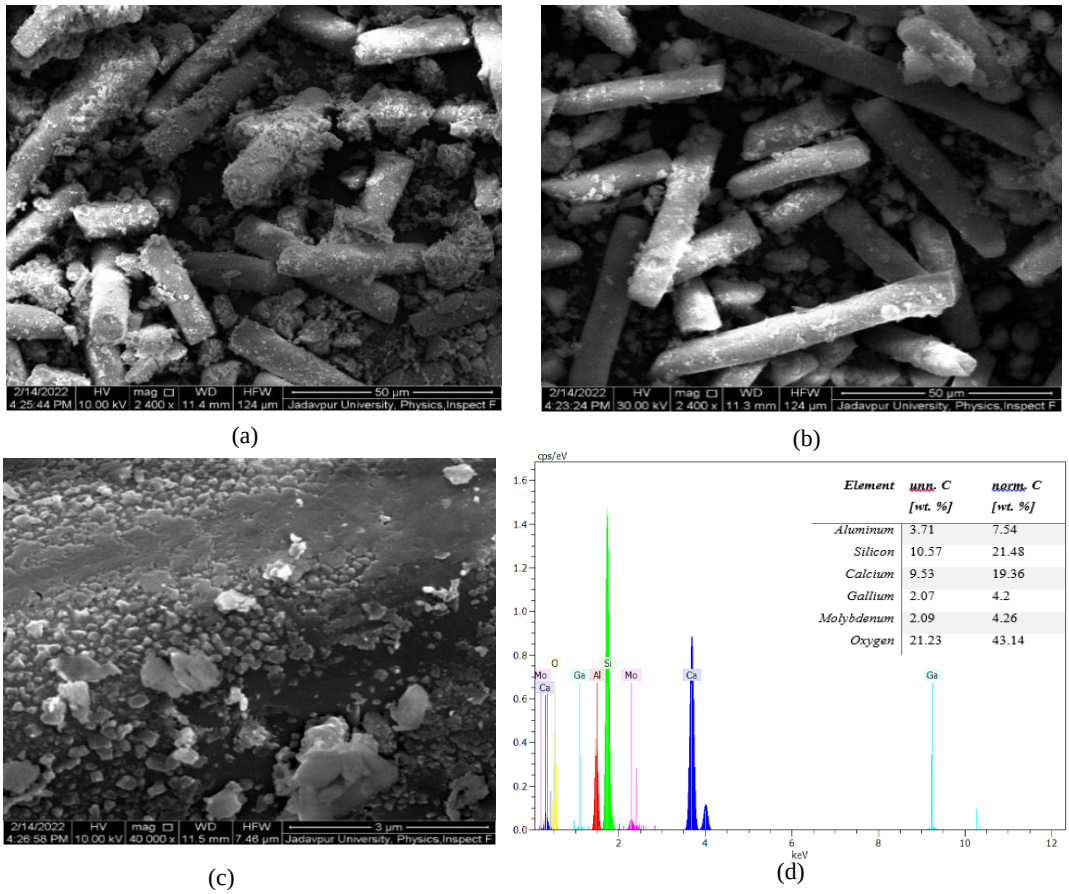

Figure 17. FESEM images of (a) non-treated GF support (b) & (c) optimum GaMo-GF catalyst (d) EDAX of optimum GaMo-GF catalyst

the EDAX analysis of all the elements along with their normalized weight percent of the optimum photo-catalyst is depicted in Figure 17(d).

7.9 High-resolution transmission electron microscopy (HRTEM)

HRTEM analysis was carried out in order to understand the structure better as seen in Figure 18. ImageJ software has been used to measure the impregnated metal crystallite sizes which confirms the nano impregnation of MoO_3 and GaON on GF support. The measured crystallite sizes for MoO_3 and GaON were 7.24 & 22.147 nm respectively (which is further confrimed from the calculated XRD data). The d-spacing of the catalyst has also been evaluated. As seen from Figure 18 the d-spacing of 0.328nm confirms the (110 plane) of orthorhombic MoO_3 phase [92] and 0.475nm corresponds to the d-spacing of gallium[93].

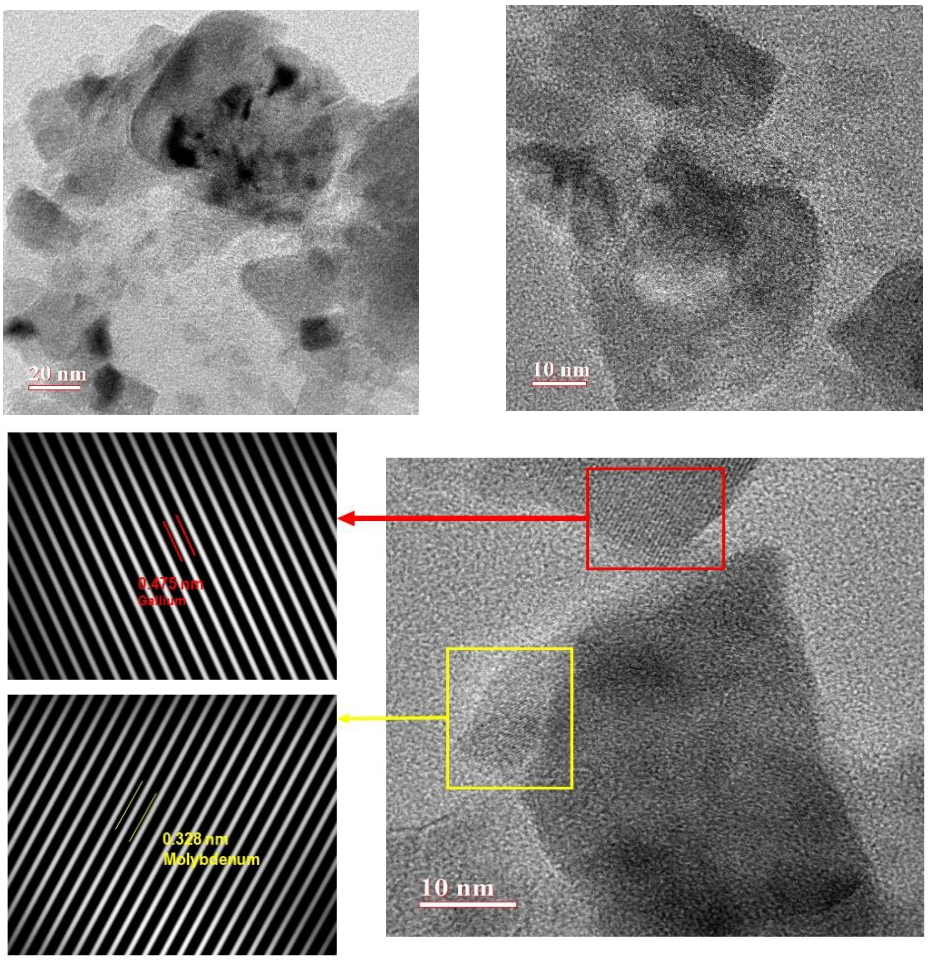

Figure 18: HRTEM images of optimum catalyst

7.10 Brunauer-Emmett-Teller (BET)

The specific surface area of both the catalyst and the support were determined using BrunauerEmmettTeller (BET) studies of the catalyst support and the generated optimum GaMo-GF photocatalyst (Table 8). After calcination, the best GaMo-GF photocatalyst had a surface area of 28.008 m^2/gm which is much greater than 20.25 m^2/gm than the W-PCB-derived silica-alumina support. The bulk of the oxides, nitrates as well as organic matter are evaporated during calcination, which results in the opening of numerous pores, increasing the photocatalyst's surface area. The investigation revealed that the samples' total pore volume and pore diameter were both mesoporous. It is suggested that the isotherm is convex to the (P/P_0) axis can describe type III of the IUPAC classification based on the form of the isotherm. Figure 19 indicating pore volume of the ideal catalyst like a function of P/P_0. Adsorbate-adsorbate interactions are indicated by an isotherm of this kind. The mesoporous property of the ideal catalyst is supported by the thin layer of hysteresis that typically occurs in the multilayered range (P/P_0 range of 0.578 to 0.87) of isotherms and is related with capillary condensation in mesoporous structures.

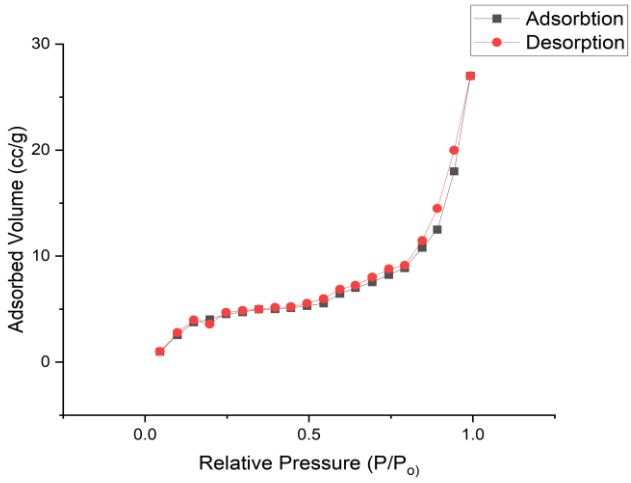

Figure 19: BET Isotherm of the optimum GaMo-GF catalyst

Table 8: BET analysis of GF support and GaMo-GF catalyst

Sample	Surface Area (m^2/g)	Total pore volume (cc/g)	Pore diameter (nm)
GF support	20.25	0.03194	11.896
GaMo-GF catalyst	28.008	0.04198	13.5872

7.11 Ammonia TPD

According to NH_3-TPD analyses of the prepared optimum GaMo-GF catalyst (Figure 20), each of the catalysts was distributed with some weak (signal maxima at 175-225°C) and strong (signal maxima at 325-375 °C) acidic sites over the temperature range of 100-550 °C. Additionally, it was possible to see that the NH_3 desorption peak was enhanced in the higher temperature zone with an increase in gallium precursor loading while showing lower peaks in the lower temperature zone which is in accordance with previous studies [94]. This was due to the partial replacement of aluminium with gallium which increases the Lewis acid sites (high-temperature zone).

Moreover, as depicted in Figure 20, low-temperature weak acid sites were also present, which enhanced the RS yield.

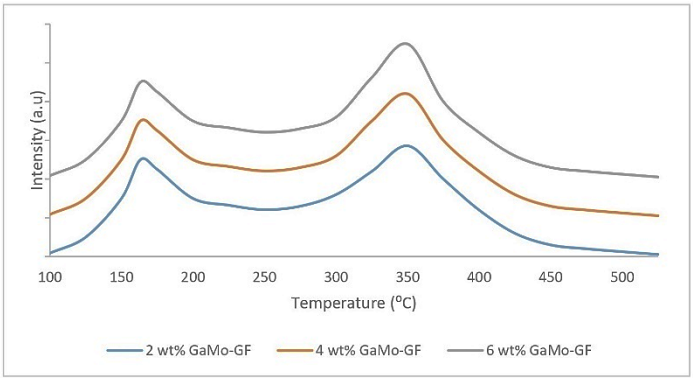

Figure 20. NH_3TPD of the synthesized GaMo-GF catalyst

7.12 UV-Vis-NIR Spectroscopy

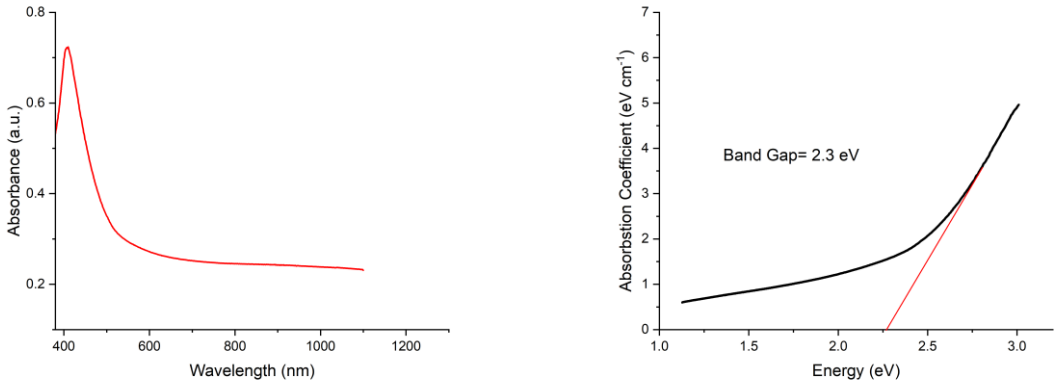

(a) **(b)**

Figure 21: (a) Absorbance spectra of optimal GaMo-GF catalyst. (b) Tauc plot of optimal GaMo-GF catalyst

The optimal GaMo-GF catalyst's UV-Vis-NIR spectrophotometric measurement (Figure 21 (a)) revealed a sizable absorbance peak in wavelength range of 400-550 nm (in the visible light range), showing the existence of GaON[90] in the generated photocatalyst. The margins of the absorption bands between 400 and 550 nm show that visible light may excite electrons in GaMo-GF catalysts to move from the valence band to the conduction band. There was no absorbance peak in the 600-800nm wavelength

range which indicates the complete absence of copper[95]. Using the Kubelka-Munk equation and the Tauc plot, a band gap energy (Eg = 2.3 eV) of GaMo-GF was calculated from reflectance spectra (Figure 21 (b))

7.13 Catalyst Reusibility

Eight successive sets of experiments at the optimum photocatalytic hydrolysis of DCC condition were used to assess the reusability of said developed optimum catalyst GaMo-GF. The catalyst was easily recovered out from photohydrolysis residue using screening (mesh size: 250), which was used in subsequent photocatlytic-hydrolysis stage after being hot air dried for 2 hours at 105°C. The RS yield droped from 72.47% to 67.14% after the 6th run due to partial leaching of Mo (0.12ppm) which was found from ICP (Inductively coupled plasma) analysis of the reused catalyst, this is line with the findings of Zhao et al.49. No further decrease in yeild was observed upto 8th run.

7.14 Life-cycle impact assessment

The results of the environmental impact assessment utilizing ReCiPe Midpoint (H) v1.11 are depicted in Figure 13 & Figure 14. The LCA data for different process are tabluted in Table 9 to Table 15. The findings showed that the main midway impact indicators for all three system borders comprised of climate change (GWE100), fossil depletion (FSD), human toxicity (HTL), ionising radiation (IR_HE), metal depletion (MeDP), and water depletion (WaDP). The GaMo-GF catalyzed photocatalytic hydrolysis of PCC in QHSR resulted in less impacts in all categories in comparison to catalytic hydrolysis in THR, as shown in Figure 22(a), which compares environmental effects of catalytic reaction in both types of reactor. The GWE100 was reduced by 57.7%, FSD by 59.9% & WaDP by 53.4% by using radiation heated reactor over traditionally heated rector. Additionally Figure 23(a & b) demonstrates that the corncob

delignification process (62.61-83.15% in QHSR & 82.55-93.32% in THR) especially the use of huge amount of acetic acid (49.12-75.99% in QHSR & 54.12-85.29% in THR) is the highest contributor to GWE100, FSD, IR_HE and WaDP, where as catalyst preparation (87.79-93.1% in QHSR & 73.75-83.49% in THR) was the main contributor for HTL and MeDP. The use of metal precurssors is the primary reason for highest contribution of catalyst prepration. Additionally, compared to using fresh catalyst, the DCC photocatalytic-hydrolysis method with its 8 cycles of catalyst recycling has less of an impact on the environment (Figure 22(b)).

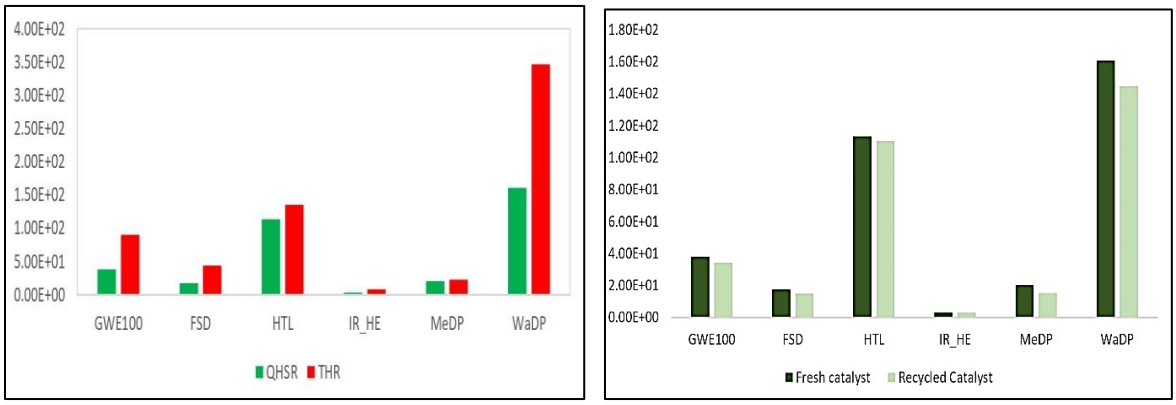

(a) **(b)**

Figure 22: (a) Comparative environmental impacts of QHSR and THR. (b) Comparative environmental impact analysis of recycled catalyst over fresh catalyst

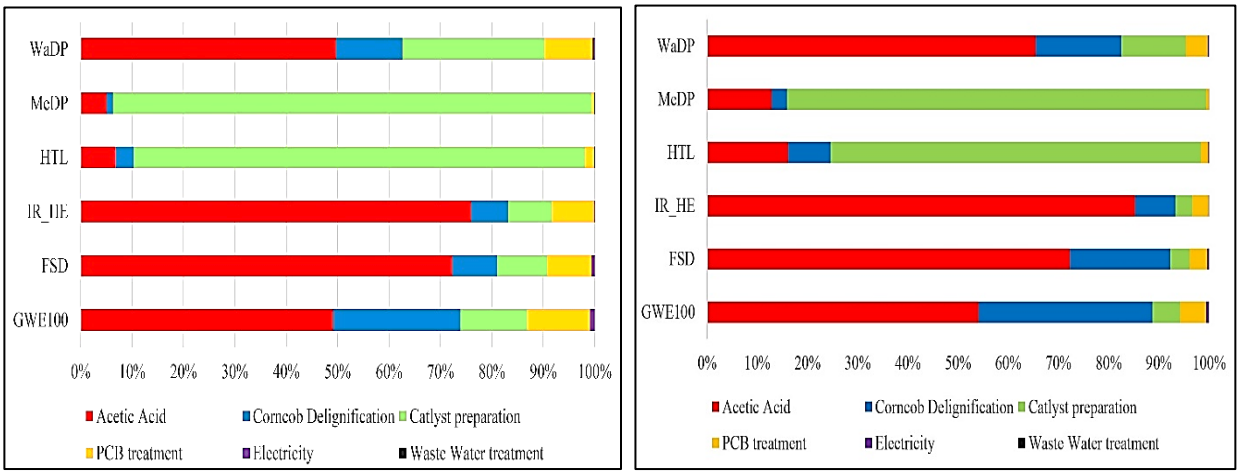

(a) **(b)**

Figure 23: (a) Relative percentage contribution of different sub processes for QHSR. (b) Relative percentage contribution of different sub processes for THR

The energy required to yield 72.47% RS from DCC in QHSR (200W, 20mins) is 240kJ, while to produce ~70% RS in THR (600W, 120mins), the energy required was 4320kJ. Hence the QHSR is more than 90% energy efficient than THR. Moreover, the cost analysis of the W-PCB extraction and optimum GaMo-GF catalyst preparation was conducted. The silica-alumina derived from W-PCB cost INR 37.63 per kg, whereas the commercial silica-alumnia cost INR 475/kg. The estimated cost of 1kg GaMo-GF catalyst preparation and 1kg of RS synthesis were INR 388.85 and INR 321.78, respectively. Furthermore, compared to the previous study[96], the cost of optimum GaMo-GF catalyst required (INR 72.33) for producing 1kg of reducing sugar was much less (INR 219, when Amberlyst 15 was used).

Table 9: LCI data for preparation of 1 kg powdered W-PCB powder					
Category	**Flow**	**Value**	**Unit**	**Source**	**Comments**
Energy Input	Electricity	0.4987	KWh	Ecoinvent v3.8	
Material Input	W-PCB	1.0097	Kg	Ecoinvent v3.8	
Emissions to air	Waste Heat	1.79532	MJ	Ecoinvent v3.8	Assuming all electrical energy dissipated as heat to air (1 KWh =3.6 MJ)
	Particulates <10µm	0.0097	Kg	Ecoinvent v3.8	Calculated on based of ref. [97]
Transports	W-PCB	6.25E-5	Kg* Km	Ecoinvent v3.8	Transport by lorry, capacity: 16 metric ton, EURO IV / BS IV
Output	Powdered W-PCB	1	kg	Created	

Table 10: LCI data for treatment of 0.3 kg powdered W-PCB powder					
Category	**Flow**	**Value**	**Unit**	**Source**	**Comments**
Energy Input	Energy consumed		KWh	Ecoinvent v3.8	
	For magnetic stirring	0.05			

	During peroxy acetic acid treatment	0.2			
	During ultrasonication	0.1875			
	For Oven drying	0.8			
	Total energy	**1.2375**			
Material Input	Powdered PCB	1	kg	Ecoinvent v3.8	
	NaOH	0.8	kg	Ecoinvent v3.8	
	DMF	0.1878	kg	Ecoinvent v3.8	
	Acetic Acid	0.12	kg	Ecoinvent v3.8	
	H_2O_2	0.066	kg	Ecoinvent v3.8	
	DI Water	5.25	kg	Ecoinvent v3.8	
Emissions to air	Waste Heat	4.455	MJ	Ecoinvent v3.8	Assuming all electrical energy dissipated as heat to air (1 KWh =3.6 MJ)
	Water Vapour	0.148	Kg	Ecoinvent v3.8	

Transports	NaOH	0.00005	Kg*Km	Ecoinvent v3.8	
	DMF	0.0000117	Kg*Km	Ecoinvent v3.8	
	Acetic Acid	0.0000075	Kg*Km	Ecoinvent v3.8	
	H_2O_2	0.0000 04125	Kg*Km	Ecoinvent v3.8	
	DI Water	0.0003 28125	Kg*Km	Ecoinvent v3.8	
Waste of Materials	Waste Water	6.425	Kg	Ecoinvent v3.8	
Output	Glass Fiber	0.3	Kg	Created	
	Copper Acetate	0.19	Kg	Created	
	Iron Scrap	0.0079	Kg	Created	

Table 11: LCI data for preparation of 1 kg Ga-Mo-GF[4] catalyst

Category	Flow	Value	Unit	Source	Comments
Energy Input	Traditional heating	0.067	KWh	Ecoinvent 3.8	
	Ultra-sonication	0.125	KWh	Ecoinvent 3.8	
	Calcination	2	KWh	Ecoinvent 3.8	
	Oven drying	0.4	KWh	Ecoinvent 3.8	
Material Input	Treated PCB	1.612	kg	Ecoinvent 3.8	Assuming 38% loss as per TGA data

	Gallium (III) nitrate hydrate	0.1184	Kg	Ecoinvent 3.8	
	Dioxomolybdenum (VI)	0.10967	Kg	Ecoinvent 3.8	
	Acetone	0.78	kg	Ecoinvent 3.8	
	Ammonium Hydroxide	0.0257	kg	Ecoinvent 3.8	
Emissions to air	Waste Heat	3.4272	MJ	Ecoinvent 3.8	Assuming all electrical energy dissipated as heat to air (1 KWh =3.6 MJ)
	Acetone	0.5	Kg	Ecoinvent 3.8	
Transport	Gallium (III) nitrate hydrate	0.0000074	Kg*Km	Ecoinvent 3.8	
	Dioxomolybdenum (VI)	0.00000685	Kg*Km	Ecoinvent 3.8	
	Acetone	0.00004875	Kg*Km	Ecoinvent 3.8	
	Ammonium Hydroxide	0.0000016	Kg*Km	Ecoinvent 3.8	
Waste of Material	Acetone	0.28	Kg	Ecoinvent 3.8	
Output	Ga-Mo-GF catalyst	1	Kg	Created	

Table 12: LCI data for 1kg powdered corncob production					
Category	**Flow**	**Value**	**Unit**	**Source**	**Comments**
Energy Input	Electricity Consumed	0.55	KWh	Ecoinvent v3.8	
Material Input	Corn Cob	1	kg	Ecoinvent v3.8	
Emission To Air	Waste Heat	1.98	MJ	Ecoinvent v3.8	Assuming all electrical energy dissipated as heat to air (1 KWh =3.6 MJ)
Transports	Corn cob	0.0000625	Kg*Km	Ecoinvent v3.8	
Output	Powdered Corncob	1	Kg		

Table 13: LCI data for delignification of 1kg of corncob					
Category	**Flow**	**Value**	**Unit**	**Source**	**Comments**
Energy Input	Electricity Consumed		kWh	Ecoinvent v3.8	
	Magnetic stirring and heating	0.3	kWh	Ecoinvent v3.8	
	Ultra-sonication	0.125	kWh	Ecoinvent v3.8	
	Hot air oven	0.109	kWh	Ecoinvent v3.8	

	Total	0.534	kWh	Ecoinvent v3.8	
Material Input	Powdered Corncob	1	Kg	Created	
	Acetic Acid (98%)	2.36	Kg	Ecoinvent v3.8	
	H_2O_2 (50%)	0.29925	Kg	Ecoinvent v3.8	
	DI water	4.5	Kg	Ecoinvent v3.8	
Emission to air	Waste Heat	1.9224	MJ	Ecoinvent v3.8	Assuming all electrical energy dissipated as heat to air (1 KWh =3.6 MJ)
	Water Vapour	1	Kg	Ecoinvent v3.8	
Transport	Acetic Acid (98%)	0.000147	Kg*Km	Ecoinvent v3.8	
	H_2O_2 (50%)	0.000187	Kg*Km	Ecoinvent v3.8	
	DI water	0.000281	Kg*Km	Ecoinvent v3.8	
Waste of Material	Waste Water	6.15925	Kg	Ecoinvent v3.8	
Output	cellulose	0.3354	Kg	Ecoinvent v3.8	
	Hemicellulose	0.2218	Kg	Ecoinvent v3.8	
	Total Holo-Cellulose	**0.5572**	kg	Ecoinvent v3.8	

Table 14: LCI data for 1kg RS production using QHSR					
Category	**Flow**	**Value**	**Unit**	**Source**	**Comments**
Energy Input	Electricity Consumption				
	For heating	0.083	kWh	Ecoinvent v3.8	(assuming 100W for each bulb)
	Stirring	0.028	kWh	Ecoinvent v3.8	
	Vacuum evaporation	0.1	kWh	Ecoinvent v3.8	
	Total	0.111	kWh		
Material Input	Holocellulose	1.24	Kg	Ecoinvent v3.8	
	Distilled water	10	kg	Ecoinvent v3.8	Considering 90% water recycling after product separation through vacuum evaporation
	GaMo-GF catalyst	0.186	Kg	Created	
Emission to air	Waste heat	0.3996	MJ	Ecoinvent v3.8	Assuming all electrical energy dissipated as heat to air (1 KWh =3.6 MJ)
Waste of Material	Waste water	5	kg	Ecoinvent v3.8	Water with produced Humin
Output	Reducing Sugar	1	kg	Created	

Table 15: LCI data for 1kg RS production using THR (conventional)					
Category	**Flow**	**Value**	**Unit**	**Source**	**Comments**
Energy Input	Electricity consumption			Ecoinvent v3.8	
	For heating	0.2	kWh		600W heater
	For stirring	0.028	kWh		
	Vacuum evaporation	0.1	kWh		
	Total	**0.228**	KWh		
Material Input	Holocellulose	3.518	Kg	Ecoinvent v3.8	
	Distilled Water	10	Kg	Ecoinvent v3.8	Considering 90% water recycling after product separation through vacuum evaporation
	Ga-Mo-GF catalyst	0.186	Kg	Ecoinvent v3.8	
Emission to air	Waste Heat	0.8208	MJ	Ecoinvent v3.8	Assuming all electrical energy dissipated as heat to air (1 KWh =3.6 MJ)

Waste material	Waste water	7.518	Kg	Ecoinvent v3.8	Water with produced Humin
Output	Reducing Sugar	1	Kg	Ecoinvent v3.8	

7.15 Comparative study

A comparison of current research to previously published studies has been conducted and presented in Table 16. It has been observed that to produce reducing sugars from cellulose or other biomasses mostly requires severe reaction condionts. Though use of microwave irradiation (1200W)[48,49] gives higher yield at a less severe rection condition the energy consuption is very high. Where as, photocatalytic hydrolysis of DCC under quartz halogen radiation (250W) has milder reaction conditions, comparitively higher yield and consumes a lot less energy. Hence the current study may be a more sustainable process.

Table 16: Comparitive study of RS production to the current study

Feedstock	**Catalyst**	**Temperature (ºC)**	**Time (hrs)**	**Yield (%)**	**Remarks**
Cellulose	BC-SO_3H[48]	90	1	24.1	• Microwave assisted reaction. • Reaction time very high. • Microwave consumes a huge amount of energy. • Low yield
Cellulose	Au-HYT[98]	140	16	58.7	• Under visible light radiation.

					• Very severe reaction conditions.
Corncob	CSA[49]	130	1	34.6	• Microwave reactor hence high energy consumption. • Low yield • High reaction temperature and time.
Cellulose	CP-SO_3H[50]	120	10	91	• Traditional heating hence greater environmental impacts. • High yield but at the cost of severe reaction conditions.
Cellulose	[C_4mim]Cl + HY[99]	100	0.25	34.8	• Microwave heating hence very high energy consumption. • Low yield at high temperature.
	[C_4mim]Cl + HZSM		0.167 (10 min)	42.9	
Cellulose	[BMIm]Cl + HY[100]	130	0.5	68.2	• Conventional heating hence high energy consumption. • Severe reaction condition.

a= in this study

Chapter 8

CONCLUSION

Conclusion

The silica-alumina support derived from W-PCB can be utilized to make gallium-molybdenum grafted (GaMo-GF) photocatalyst. The results of the experiment unambigously demonstrated that the synthesized catalyst worked better under radiated heated reactor (72.47% RS yield) compared to its traditional counterpart (25.58% RS yield). Moreover the RS yield was much higher under milder reaction conditions when compared to previously reported studies. Furthermore, the catalyst reusability for 8 consecutive cycles in the DCC photocatalytic-hydrolysis method revealed to have a lower environmental effect than fresh catalyst. The GaMo-GF catalysed photo-hydrolysis method is also ecologically sustainable, according to an LCA studies that examined the process' overall sustainability. The QHSR based reaction showed over 50% lower environmental impact than reactions in THR. By effectively recycling comparable e-waste for the synthesis of RS for later bioethanol synthesis, the results of this study are anticipated to stimulate the growth of other potentially effective photocatalysts. Moreover, it is possible to manufacture reusable, highly effective supported acid catalyst using discarded PCBs, opening up another another efficient route for e-waste valorization and the production of value-added chemicals from LB.

Chapter 9

REFERENCES

1. Mookherjee, P. The Implications of India's Revised Roadmap for Biofuels: A Lifecycle Perspective. *ORF Issue Br.* **526**, 0–12 (2022).

2. Chandra, A. & Rosmann, M. Report Name : Biofuels Annual Table of Contents. **IN2021-007**, 1–45 (2021).

3. Corma Canos, A., Iborra, S. & Velty, A. Chemical routes for the transformation of biomass into chemicals. *Chem. Rev.* **107**, 2411–2502 (2007).

4. Zoghlami, A. & Paës, G. Lignocellulosic Biomass: Understanding Recalcitrance and Predicting Hydrolysis. *Front. Chem.* **7**, (2019).

5. Lynd, L. R. *et al.* Art ices Fuel Ethanol from Cellulosic Biomass. *Science (80-.).* **251**, 1318–1323 (2017).

6. Demirbas, A. Biofuels securing the planet's future energy needs. *Energy Convers. Manag.* **50**, 2239–2249 (2009).

7. Scheller, H. V. & Ulvskov, P. Hemicelluloses. *Annu. Rev. Plant Biol.* **61**, 263–289 (2010).

8. Keogh, G. F. *et al.* Randomized controlled crossover study of the effect of a highly β-glucan-enriched barley on cardiovascular disease risk factors in mildly hypercholesterolemic men. *Am. J. Clin. Nutr.* **78**, 711–718 (2003).

9. Ksibi, M. *et al.* Photodegradation of lignin from black liquor using a UV/TiO2 system. *J. Photochem. Photobiol. A Chem.* **154**, 211–218 (2003).

10. Sindhu, R. *et al.* Dilute acid pretreatment and enzymatic saccharification of sugarcane tops for bioethanol production. *Bioresour. Technol.* **102**, 10915–10921 (2011).

11. Sarkar, N., Ghosh, S. K., Bannerjee, S. & Aikat, K. Bioethanol production from agricultural wastes: An overview. *Renewable Energy* vol. 37 19–27 (2012).

12. de Souza, A. P., Leite, D. C. C., Pattathil, S., Hahn, M. G. & Buckeridge, M. S. Composition and Structure of Sugarcane Cell Wall Polysaccharides: Implications for Second-Generation Bioethanol Production. *Bioenergy Res.* **6**, 564–579 (2013).

13. Umagiliyage, A. L., Choudhary, R., Liang, Y., Haddock, J. & Watson, D. G. Laboratory scale optimization of alkali pretreatment for improving enzymatic hydrolysis of sweet sorghum bagasse. *Ind. Crops Prod.* **74**, 977–986 (2015).

14. Idania Valdez-Vazquez, Marisol Pérez-Rangel, Adán Tapia, Germán Buitrón, Carlos Molina, Gustavo Hernández, L. A.-D. Hydrogen and butanol production from native wheat straw by synthetic microbial consortia integrated by species of Enterococcus and Clostridium, Fuel. *Fuel* **159**, 214–222 (2015).

15. Bevilaqua, D. B., Rambo, M. K. D., Rizzetti, T. M., Cardoso, A. L. & Martins, A. F. Cleaner production: Levulinic acid from rice husks. *J. Clean. Prod.* **47**, 96–101 (2013).

16. Gonda, S., Kiss-Szikszai, A., Szűcs, Z., Balla, B. & Vasas, G. Efficient biotransformation of non-steroid anti-inflammatory drugs by endophytic and epiphytic fungi from dried leaves of a medicinal plant, Plantago lanceolata L., International Biodeterioration & Biodegradation. *Int. Biodeterior. Biodegradation* **108**, 115–121 (2016).

17. Zhi, Z. *et al.* Kinetic study of levulinic acid production from corn stalk at relatively high temperature using FeCl3 as catalyst: A simplified model

evaluated. *Ind. Crops Prod.* **76**, 672–680 (2015).

18. Zhao, P., Zhou, C., Li, J., Xu, S. & Hu, C. Synergistic Effect of Different Species in Stannic Chloride Solution on the Production of Levulinic Acid from Biomass. *ACS Sustain. Chem. Eng.* **7**, 5176–5183 (2019).

19. Qing, Q. *et al.* Kinetics study of levulinic acid production from corncobs by tin tetrachloride as catalyst. *Bioresour. Technol.* **260**, 150–156 (2018).

20. Theander, O. Cellulose, Hemicellulose and Extractives. *Fundam. Thermochem. Biomass Convers.* 35–60 (1985) doi:10.1007/978-94-009-4932-4_2.

21. Brosse, N., Dufour, A., Meng, X., Sun, Q. & Ragauskas, A. Miscanthus: a fast-growing crop for biofuels and chemicals production Nicolas. *Biofuels, Bioprod. Biorefining* **6**, 246–256 (2012).

22. Forti, V., Baldé, C. P., Kuehr, R. & Bel, G. *The Global E-waste Monitor 2020*. (2020).

23. Shen, Y. *et al.* Waste-to-energy: Dehalogenation of plastic-containing wastes. *Waste Manag.* **49**, 287–303 (2016).

24. Cesaro, A., Marra, A., Belgiorno, V. & Guida, M. Effectiveness of WEEE mechanical treatment: Separation yields and recovered material toxicity. *J. Clean. Prod.* **142**, 2656–2662 (2017).

25. Oguchi, M., Sakanakura, H. & Terazono, A. Toxic metals in WEEE: Characterization and substance flow analysis in waste treatment processes. *Sci. Total Environ.* **463**–**464**, 1124–1132 (2013).

26. Wang, C., Wang, H. & Cao, Y. Waste printed circuit boards as novel potential engineered catalyst for catalytic degradation of orange II. *J. Clean. Prod.* **221**,

234–241 (2019).

27. Yoo, J. M., Jeong, J., Yoo, K., Lee, J. chun & Kim, W. Enrichment of the metallic components from waste printed circuit boards by a mechanical separation process using a stamp mill. *Waste Manag.* **29**, 1132–1137 (2009).

28. Jie, G., Ying-Shun, L. & Mai-Xi, L. Product characterization of waste printed circuit board by pyrolysis. *J. Anal. Appl. Pyrolysis* **83**, 185–189 (2008).

29. Zhang, S., Yoshikawa, K., Nakagome, H. & Kamo, T. Steam gasification of epoxy circuit board in the presence of carbonates. *J. Mater. Cycles Waste Manag.* **14**, 294–300 (2012).

30. Havlik, T., Orac, D., Berwanger, M. & Maul, A. The effect of mechanical-physical pretreatment on hydrometallurgical extraction of copper and tin in residue from printed circuit boards from used consumer equipment. *Miner. Eng.* **65**, 163–171 (2014).

31. Yang, J. G., Wu, Y. T. & Li, J. Recovery of ultrafine copper particles from metal components of waste printed circuit boards. *Hydrometallurgy* **121**–**124**, 1–6 (2012).

32. Greenwood, N., N. & Earnshaw, A. Chemistry of the Elements. Oxford: Pergamon Press. (1984) doi:ISBN 0-08-022057-6.

33. Kurtoglu, M. E., Longenbach, T. & Gogotsi, Y. Preventing Sodium Poisoning of Photocatalytic TiO2 Films on Glass by Metal Doping. *Int. J. Appl. Glas. Sci.* **2**, 108–116 (2011).

34. FUJISHIMA, A. & HONDA, K. Electrochemical Photolysis of Water at a Semiconductor Electrode. **238**, 37–38 (1972).

35. Pal, R. Amberlyst-15 in Organic Synthesis Amberlyst-15 in organic synthesis. *Arch. Org. Chem.* **2012**, 570–609 (2015).

36. Onda, A., Ochi, T. & Yanagisawa, K. Selective hydrolysis of cellulose into glucose over solid acid catalysts †. *Green Chem.* **10**, 1033–1037 (2008).

37. Li, X., Peng, K., Xia, Q., Liu, X. & Wang, Y. Efficient conversion of cellulose into 5-hydroxymethylfurfural over niobia/carbon composites. *Chem. Eng. J.* **332**, 528–536 (2018).

38. Charisteidis, I. D. & Triantafyllidis, K. S. Propylene epoxidation by molecular oxygen using supported silver catalysts: Effect of support type, preparation method and promotion with alkali chloride and/or steam. *Catal. Today* **355**, 654–664 (2020).

39. Kappe, C. O., Pieber, B. & Dallinger, D. Microwave effects in organic synthesis: Myth or reality? *Angew. Chemie - Int. Ed.* **52**, 1088–1094 (2013).

40. Dudley, G. B., Richert, R. & Stiegman, A. E. On the existence of and mechanism for microwave-specific reaction rate enhancement. *Chem. Sci.* **6**, 2144–2152 (2015).

41. Camesasca, L., Ramírez, M. B., Guigou, M., Ferrari, M. D. & Lareo, C. Evaluation of dilute acid and alkaline pretreatments, enzymatic hydrolysis and fermentation of napiergrass for fuel ethanol production. *Biomass and Bioenergy* **74**, 193–201 (2015).

42. Liu, C., Wang, H., Karim, A. M., Sun, J. & Wang, Y. Catalytic fast pyrolysis of lignocellulosic biomass. *Chem. Soc. Rev.* **43**, 7594–7623 (2014).

43. Mittal, A., Pilath, H. M. & Johnson, D. K. Direct Conversion of Biomass

Carbohydrates to Platform Chemicals: 5 - Hydroxymethylfurfural (HMF) and Furfural. *Energy Fuels* **34**, 3284–3293 (2020).

44. Hermiati, E., Tsubaki, S. & Azuma, J. Cassava Pulp Hydrolysis under Microwave Irradiation with Oxalic Acid Catalyst for Ethanol Production. *J. Math. Fund. Sci.* **46**, 125–139 (2014).

45. Lenihan, P. *et al.* Dilute acid hydrolysis of lignocellulosic biomass. *Chem. En* **156**, 395–403 (2009).

46. Kupiainen, L., Ahola, J. & Tanskanen, J. Hydrolysis of organosolv wheat pulp in formic acid at high temperature for glucose production. *Bioresour. Technol.* **116**, 29–35 (2012).

47. Yu, H. *et al.* Enhanced enzymatic hydrolysis of cellulose from waste paper fibers by cationic polymers addition. *Carbohydr. Polym.* **200**, 248–254 (2018).

48. Wu, Y. *et al.* Microwave-assisted hydrolysis of crystalline cellulose catalyzed by biomass char sulfonic acids. *Green Chem.* **12**, 696–700 (2010).

49. Jiang, Y. *et al.* Effective saccharification of lignocellulosic biomass over hydrolysis residue derived solid acid under microwave irradiation †. *Green Chem.* **14**, 2162–2167 (2012).

50. Shuai, L. & Pan, X. Hydrolysis of cellulose by cellulase-mimetic solid catalyst. *Energy Environ. Sci.* **5**, 6889–6894 (2012).

51. Juan Tian, Fan, C., Cheng, M. & Wang, X. Hydrolysis of Cellulose over Cs x H 3 – x PW 12 O 40 (X = 1 – 3) Heteropoly Acid Catalysts. *Chem. Eng. Technol.* **34**, 482–486 (2011).

52. Chatterjee, S., Barman, S. & Chakraborty, R. Combined Effects of Ionic Liquid

and Tungsten–Halogen Radiation on Heterogeneous Hydrolysis Kinetics of Waste Papaya Epidermis for Production of Total Reducing Sugar. *Waste and Biomass Valorization* **10**, 1845–1855 (2019).

53. Qi, B., Vu, A., Wickramasinghe, S. R. & Qianc, X. Biomass and Bioenergy Glucose production from lignocellulosic biomass using a membrane-based polymeric solid acid catalyst. *Biomass and Bioenergy* **117**, 137–145 (2018).

54. Shen, F., Guo, T., Bai, C., Qiu, M. & Qi, X. Hydrolysis of cellulose with one-pot synthesized sulfonated carbonaceous solid acid. *Fuel Process. Technol.* **169**, 244–247 (2018).

55. Shrotri, A., Kobayashi, H. & Fukuoka, A. Cellulose Depolymerization over Heterogeneous Catalysts. *Acc. Chem. Res.* **51**, 761–768 (2018).

56. Jin, S. *et al.* A recyclable and regenerable solid acid for efficient hydrolysis of cellulose to glucose. *Biomass and Bioenergy* **138**, 105611 (2020).

57. Qu, H., Liu, B., Li, L. & Zhou, Y. A bifunctional recoverable catalyst based on phosphotungstic acid for cellulose hydrolysis to fermentable sugars. *Fuel Process. Technol.* **199**, 1–7 (2020).

58. Norgbey, E. *et al.* Unravelling the efficient use of waste lignin as a bitumen modifier for sustainable roads. *Constr. Build. Mater.* **230**, (2020).

59. Zhao, W. *et al.* Intensified levulinic acid/ester production from cassava by one-pot cascade prehydrolysis and delignification. *Appl. Energy* **204**, 1094–1100 (2017).

60. Chin, S. X., Chia, C. H., Zakaria, S., Fang, Z. & Ahmad, S. Ball milling pretreatment and diluted acid hydrolysis of oil palm empty fruit bunch (EFB)

fibres for the production of levulinic acid. *J. Taiwan Inst. Chem. Eng.* **52**, 85–92 (2015).

61. Zhao, H. *et al.* Effects of crystallinity on dilute acid hydrolysis of cellulose by cellulose ball-milling study. *Energy and Fuels* **20**, 807–811 (2006).

62. Thakkar, A. *et al.* Production of levulinic acid and biocarbon electrode material from corn stover through an integrated biorefinery process. *Fuel Process. Technol.* **213**, (2021).

63. Pielhop, T., Amgarten, J., Von Rohr, P. R. & Studer, M. H. Steam explosion pretreatment of softwood: The effect of the explosive decompression on enzymatic digestibility. *Biotechnol. Biofuels* **9**, 1–13 (2016).

64. Teymouri, F., Laureano-Perez, L., Alizadeh, H. & Dale, B. E. Optimization of the ammonia fiber explosion (AFEX) treatment parameters for enzymatic hydrolysis of corn stover. *Bioresour. Technol.* **96**, 2014–2018 (2005).

65. MacDonald, D. G. *et al.* Alkali treatment of corn stover to improve sugar production by enzymatic hydrolysis. *Biotechnol. Bioeng.* **25**, 2067–2076 (1983).

66. Mosier, N. *et al.* Features of promising technologies for pretreatment of lignocellulosic biomass. *Bioresour. Technol.* **96**, 673–686 (2005).

67. Chen, Y. W., Lee, H. V., Juan, J. C. & Phang, S. M. Production of new cellulose nanomaterial from red algae marine biomass Gelidium elegans. *Carbohydr. Polym.* **151**, 1210–1219 (2016).

68. Rahman, N. H. A., Chieng, B. W., Ibrahim, N. A. & Rahman, N. A. Extraction and characterization of cellulose nanocrystals from tea leaf waste fibers.

Polymers (Basel). **9**, 1–11 (2017).

69. Wang, Z., Yao, Z. J., Zhou, J. & Zhang, Y. Reuse of waste cotton cloth for the extraction of cellulose nanocrystals. *Carbohydr. Polym.* **157**, 945–952 (2017).

70. Moyo, T., Chirume, B. H. & Petersen, J. Assessing alternative pre-treatment methods to promote metal recovery in the leaching of printed circuit boards. *Resour. Conserv. Recycl.* **152**, 104545 (2020).

71. Watkins, D., Nuruddin, M., Hosur, M., Tcherbi-Narteh, A. & Jeelani, S. Extraction and characterization of lignin from different biomass resources. *J. Mater. Res. Technol.* **4**, 26–32 (2015).

72. Miller, G. L. Use of Dinitrosalicylic Acid Reagent for Determination of Reducing Sugar. *Anal. Chem.* **31**, 426–428 (1959).

73. International Organization for Standardization. *Environmental management: life cycle assessment; Principles and Framework. ISO* (2006).

74. Lelekakis, N., Wijaya, J., Martin, D. & Susa, D. The effect of acid accumulation in power-transformer oil on the aging rate of paper insulation. *IEEE Electr. Insul. Mag.* **30**, 19–26 (2014).

75. Sundeep, D. *et al.* Spectral characterization of mechanically synthesized MoO3-CuO nanocomposite. *Int. Nano Lett.* **6**, 119–128 (2016).

76. Iqbal, N., Khan, I., Yamani, Z. H. & Qurashi, A. Sonochemical Assisted Solvothermal Synthesis of Gallium Oxynitride Nanosheets and their Solar-Driven Photoelectrochemical Water-Splitting Applications. *Sci. Rep.* **6**, 1–11 (2016).

77. Zhang, J. *et al.* Growth and characterization of new transparent conductive

oxides single crystals β-Ga2O3: Sn. *J. Phys. Chem. Solids* **67**, 1656–1659 (2006).

78. Joni, I. M., Nulhakim, L., Vanitha, M. & Panatarani, C. Characteristics of crystalline silica (SiO2) particles prepared by simple solution method using sodium silicate (Na2SiO3) precursor. *J. Phys. Conf. Ser.* **1080**, (2018).

79. Roy, O., Roy Choudhury, S. & Chakraborty, R. Life cycle assessment of waste printed wiring board–derived Ag photocatalyst for sustainable fermentable sugar production. *Environ. Sci. Pollut. Res.* (2022) doi:10.1007/s11356-022-19726-6.

80. Liang, Y. *et al.* Synthesis and characterization of core-shell structured SiO 2 @YVO 4 :Yb 3+ ,Er 3+ microspheres. *Appl. Surf. Sci.* **258**, 3689–3694 (2012).

81. Barontini, F., Marsanich, K., Petarca, L. & Cozzani, V. Thermal degradation and decomposition products of electronic boards containing BFRs. *Ind. Eng. Chem. Res.* **44**, 4186–4199 (2005).

82. Berbenni, V. & Milanese, C. Thermal decomposition of gallium nitrate hydrate Ga (NO 3) 3× xH 2 O. *J. Therm. …* **82**, 401–407 (2005).

83. Zhou, K. *et al.* Preparation of poly(vinyl alcohol) nanocomposites with molybdenum disulfide (MoS 2): Structural characteristics and markedly enhanced properties. *RSC Adv.* **2**, 11695–11703 (2012).

84. ChristianSchramm. High temperature ATR-FTIR characterization of the interaction of polycarboxylic acids and organotrialkoxysilanes with cellulosic material. *Spectrochim. Acta Part A Mol. Biomol. Spectrosc.* **243**, (2020).

85. Poiana, M. A. *et al.* Use of ATR-FTIR spectroscopy to detect the changes in

extra virgin olive oil by adulteration with soybean oil and high temperature heat treatment. *Open Chem.* **13**, 689–698 (2015).

86. Bruice, P. Y. Beauchamp Spectroscopy Tables 1. *Org. Chem.* **2620**, A-16, A17 (2011).

87. Cheng, Y. *et al.* Structural, morphological, FTIR and photoluminescence properties of gallium oxide thin films. *J. Vac. Sci. Technol. B, Nanotechnol. Microelectron. Mater. Process. Meas. Phenom.* **32**, 03D119 (2014).

88. Khojastehnezhad, A., Moeinpour, FaridKhojastehnezhad, A., Moeinpour, F., & Vafaei, M. (2015). Molybdenum oxide supported on silica (MoO3/SiO2): An efficient and reusable catalyst for the synthesis of 1,8-dioxodecahydroacridines under solvent-free conditions. Journal of the Me, 29–35. https://doi.org/10.29356/jmcs.v59i1.11 & Vafaei, M. Molybdenum oxide supported on silica (MoO3/SiO2): An efficient and reusable catalyst for the synthesis of 1,8-dioxodecahydroacridines under solvent-free conditions. *J. Mex. Chem. Soc.* **59**, 29–35 (2015).

89. Zhao, J., Jayakumar, A. & Lee, J. M. Bifunctional Sulfonated MoO3-ZrO2 Binary Oxide Catalysts for the One-Step Synthesis of 2,5-Diformylfuran from Fructose. *ACS Sustain. Chem. Eng.* **6**, 2976–2982 (2018).

90. Hu, C. C. & Teng, H. Gallium oxynitride photocatalysts synthesized from Ga(OH)3 for water splitting under visible light irradiation. *J. Phys. Chem. C* **114**, 20100–20106 (2010).

91. Demri, B. & Muster, D. XPS study of some calcium compounds. *J. Mater. Process. Tech.* **55**, 311–314 (1995).

92. Tang, M., Nelson, A. T., Wood, E. S., Maloy, S. A. & Jiang, Y. B. Grazing incidence X-ray diffraction and transmission electron microscopy studies on the oxide formation of molybdenum in a water vapor environment. *Scr. Mater.* **120**, 49–53 (2016).

93. Shah, J., Ratnasamy, P. & Carreon, M. L. Influence of the nanostructure of gallium oxide catalysts on conversion in the green synthesis of carbamates. *Catalysts* **7**, (2017).

94. Han, Z. *et al.* Synthesis of gallium-containing ZSM-5 zeolites by the seed-induced method and catalytic performance of GaZSM-5 and AlZSM-5 during the conversion of methanol to olefins. *J. Taiwan Inst. Chem. Eng.* **103**, 149–159 (2019).

95. Yoong, L. S., Chong, F. K. & Dutta, B. K. Development of copper-doped TiO2 photocatalyst for hydrogen production under visible light. *Energy* **34**, 1652–1661 (2009).

96. Chatterjee, S., Barman, S. & Chakraborty, R. Far infrared radiated energy-proficient rapid one-pot green hydrolysis of waste watermelon peel: Optimization and heterogeneous kinetics of glucose synthesis. *RSC Adv.* **6**, 74278–74287 (2016).

97. Xue, M., Yang, Y., Ruan, J. & Xu, Z. Assessment of noise and heavy metals (Cr, Cu, Cd, Pb) in the ambience of the production line for recycling waste printed circuit boards. *Environ. Sci. Technol.* **46**, 494–499 (2012).

98. Wang, L. *et al.* Sustainable conversion of cellulosic biomass to chemicals under visible-light irradiation. *RSC Adv.* **5**, 85242–85247 (2015).

99. Zhang, Z. & Zhao, Z. K. Solid acid and microwave-assisted hydrolysis of cellulose in ionic liquid. *Carbohydr. Res.* **344**, 2069–2072 (2009).

100. Cai, H., Li, C., Wang, A., Xu, G. & Zhang, T. Zeolite-promoted hydrolysis of cellulose in ionic liquid, insight into the mutual behavior of zeolite, cellulose and ionic liquid. *Appl. Catal. B Environ.* **123**–**124**, 333–338 (2012).

Appendix-I

Appendix-II

Name of Tables